



Cassiterite oxygen isotopes in magmatic-hydrothermal systems: in situ microanalysis, fractionation factor, and applications

Yang Li¹ · Sheng He² · Rong-Qing Zhang³ · Xian-Wu Bi⁴ · Lian-Jun Feng¹ · Guo-Qiang Tang¹ · Wen-Zhong Wang^{5,6} · Fang Huang⁷ · Xian-Hua Li¹

Received: 18 February 2021 / Accepted: 3 July 2021

© The Author(s), under exclusive licence to Springer-Verlag GmbH Germany, part of Springer Nature 2021

Abstract

Tin and tungsten are important metals for the industrializing society. Deciphering the origin and evolution of hydrothermal fluids responsible for their formation is critical to underpin genetic models of ore formation. Traditional approaches obtain isotopic information mainly from bulk analysis of both ore and gangue minerals, or less frequently from in situ analysis of gangue minerals, which either bear inherited complexities and uncertainties or are indirect constraints. Hence, directly obtaining isotopic information from ore minerals such as cassiterite by in situ techniques is warranted. However, this has been hampered by challenges from both analytical and applicational aspects. In this study, we first demonstrate a lack of crystallographic orientation effects during cassiterite ion microprobe oxygen isotope analysis. Along with our newly developed matrix-matched reference material, the Yongde-Cst, which has a recommended $\delta^{18}\text{O}$ value of $1.36 \pm 0.16\%$ (VSMOW) as defined by gas source isotope ratio mass spectrometry, in situ oxygen isotope analysis of cassiterite now is possible. We further refine the oxygen isotope fractionation ($1000 \ln \alpha$) for quartz-cassiterite by first-principles calculations, which is given by the equation of $1.259 \times 10^6/T^2 + 8.15 \times 10^3/T - 4.72$ (T is temperature in Kelvin). The $1000 \ln \alpha$ for quartz-cassiterite has a sensitive response to temperature, and makes cassiterite-quartz an excellent mineral pair in oxygen isotope thermometry, as described by the equation of T ($^{\circ}\text{C}$) = $2427 \times (\delta^{18}\text{O}_{\text{qtz}} - \delta^{18}\text{O}_{\text{cst}})^{-0.4326} - 492.4$. Using the well-established $1000 \ln \alpha$ of quartz-water, $1000 \ln \alpha$ of cassiterite-water is derived as $2.941 \times 10^6/T^2 - 11.45 \times 10^3/T + 4.72$ (T in Kelvin), which shows a weak response to temperature. This makes cassiterite an ideal mineral from which to derive $\delta^{18}\text{O}$ of fluids as robust temperature estimates are no longer a prerequisite. We have applied oxygen isotope analysis to cassiterite samples from six Sn(-W) deposits in China. The results show considerable variability in $\delta^{18}\text{O}$ values both within a single deposit and among studied deposits. Combining the $\delta^{18}\text{O}$ of cassiterite samples and the equilibrium oxygen isotope fractionation, we find that the $\delta^{18}\text{O}$ values of ore-forming fluids show a strong magmatic affinity with variable but mostly no to low degree involvements (~ 0 – 10%) of meteoric water, hence our results invite a reassessment on the extent and role of meteoric water in Sn-W mineralization. This study demonstrates that in situ oxygen isotope analysis of cassiterite is a promising tool to refine sources of ore-forming fluids, and to decode hydrothermal dynamics controlling tin and tungsten mineralization.

Keywords Reference material · Crystallographic orientation effects · Fluid mixing · Isotope thermometry · Sn(-W) deposit · Fluid source and evolution

Introduction

Tin and tungsten are mostly sourced from magmatic-hydrothermal systems and bear a specific genetic association with peraluminous granites (Lehmann 1982; Blevin and Chappell 1995; Breiter et al. 2007). Formation of these deposits requires efficient scavenging of metals from their sources into hydrothermal fluids, and then their transport to sinks for mineralization (Wood and Samson 2000; Carr et al. 2020). In this process, aqueous fluids play a critical

Editorial handling: D. Dolejs.

✉ Yang Li
geoliy@outlook.com

Extended author information available on the last page of the article

role in the mobilization, concentration, transportation, and eventually deposition of tin and tungsten. In this regard, robust constraints on the sources, nature, and evolution of hydrothermal fluids responsible for ore formation are essential for a better understanding of ore genesis. Oxygen is the most abundant element in aqueous fluids, and fluids from different origins typically bear diagnostic oxygen isotope compositions, which are a key proxy to directly decipher sources and track the evolution of ore-forming fluids (Cooke et al. 2014). Isotopic information of ore-forming fluids is predominantly obtained from two approaches. The first is bulk analysis of fluid inclusion assemblages (Bodnar et al. 2014). Fluid inclusions are remnants of paleo-fluids trapped during crystallization of gangue minerals (e.g., quartz) and ore minerals (e.g., cassiterite, wolframite). Extracting these ancient fluids for isotope analysis can give a direct measurement of the oxygen isotope composition of ore-forming fluids (Wilkinson 2001). On the other hand, both gangue minerals and ore minerals with oxygen in their crystal lattice can be analyzed via bulk analysis to obtain $\delta^{18}\text{O}$ values of minerals, with $\delta^{18}\text{O}$ values of fluids being derived using the known oxygen isotope fractionation ($1000 \ln \alpha$) between mineral and water (Clayton et al. 1972). Due to almost unavoidable risks of mixing aliquots of fluids or domains of minerals from multiple stages of mineralization, which is inherent in the nature of bulk analysis, isotopic information obtained through these conventional approaches is subject to complexities and uncertainties, so interpretation from these data can be ambiguous.

In situ oxygen isotope analysis of ore minerals by ion microprobe (i.e., CAMECA SIMS and SHRIMP SI), such as cassiterite, the principal ore mineral of tin, is a promising method to directly obtain oxygen isotope compositions from ore minerals without mixing information from multiple stages of mineral growth. In comparison to analyzing gangue minerals, analyzing ore minerals also removes the fundamental assumption that gangue minerals and ore minerals are precipitated from the same aliquot of fluids. The ability of in situ techniques to overcome the drawbacks discussed above has been partly demonstrated in its applications to gangue minerals (D'Errico et al. 2012; Fekete et al. 2016; Li et al. 2018). An additional advantage of utilizing in situ techniques with high spatial resolution is that with detailed petrographic studies, texturally controlled information in mineral grains can be translated into temporal evolution patterns to reveal crystal growth history, and to reconstruct magmatic-hydrothermal processes during mineral precipitation. Such an approach is very beneficial for hydrothermal minerals with large grain sizes, such as cassiterite from Sn(-W) deposits, and it holds the promise to reveal fluid dynamics with unprecedented detail. Ion microprobes have been available to the geological community for more than half a century and have been routinely applied to the analysis of

oxygen isotopes in silicates and carbonates. However, their applications to ore minerals are rare, and this is what we explore here.

An important consideration in ion microprobe analysis is the crystallographic orientation effect. When it is present, measured $\delta^{18}\text{O}$ values will strongly correlate with the crystallographic orientation of the analyzed mineral relative to the incoming primary ion beam (Huberty et al. 2010). Previous studies have shown that rutile, an isostructural mineral with cassiterite, shows significant crystallographic orientation effects (Schmitt and Zack 2012; Taylor et al. 2012; Shulaker et al. 2015). As such, it is reasonable to expect that cassiterite might also show a crystallographic orientation effect, and rigorous evaluation is critical to making accurate oxygen isotope analysis. Carr et al. (2017) pioneered in situ cassiterite oxygen isotope analysis by SHRIMP SI. Using cassiterite grains from the Elsemore Granite in the New England Orogen, eastern Australia, they were able to achieve a reproducibility of $\sim 2\%$. Precision at this level limits its geological applications. With the potential presence of sample heterogeneity in the Elsemore cassiterite at the $\sim 2\%$ level, as highlighted by Carr et al. (2017), it is difficult to decipher whether the $\sim 2\%$ variation in their study was caused by true oxygen isotopic heterogeneity of the Elsemore cassiterite, or the presence of crystallographic orientation effects. An additional requirement for ion microprobe analysis is correcting for instrumental mass fractionation (IMF), which is matrix-dependent. As such, to facilitate routine cassiterite oxygen isotope analysis, it is critical to conduct a rigorous evaluation of the crystallographic orientation effect, and to characterize matrix-matched reference materials.

Once the technique for cassiterite oxygen isotope analysis has been established, it is necessary to transfer $\delta^{18}\text{O}$ values of cassiterite to $\delta^{18}\text{O}$ values of fluids during cassiterite crystallization, for which knowing the temperature-dependent oxygen isotope fractionation ($1000 \ln \alpha$) between cassiterite and water is a prerequisite. Both experimental and computational approaches have been utilized to derive $1000 \ln \alpha$ (Zheng 1991; Zhang et al. 1994; Hu et al. 2005; Polyakov et al. 2005). Recent advances in first-principles calculations offer new chances to evaluate robustness of previous estimates from an independent perspective.

Once the analytical challenges and fractionation factors having been defined, it is necessary to demonstrate their application to cassiterite-bearing deposits. As a response to these challenges, here, we present a comprehensive and systematic investigation of cassiterite oxygen isotope in magmatic-hydrothermal systems. We first demonstrate a lack of crystallographic orientation effects in SIMS cassiterite oxygen isotope analysis, and then report the Yongde-Cst, the first cassiterite oxygen isotope reference material.

We further calculate $1000 \ln \alpha$ between cassiterite and quartz using the density functional theory (DFT) method, with $1000 \ln \alpha$ between cassiterite and water being calculated using $1000 \ln \alpha$ between quartz and water from Sharp et al. (2016). We finally apply our methods to cassiterite samples from six well-studied Sn(-W) deposits from a variety of geological settings. The results indicate that cassiterite oxygen isotope analysis is promising in ore-forming process studies.

Samples

The Yongde cassiterite

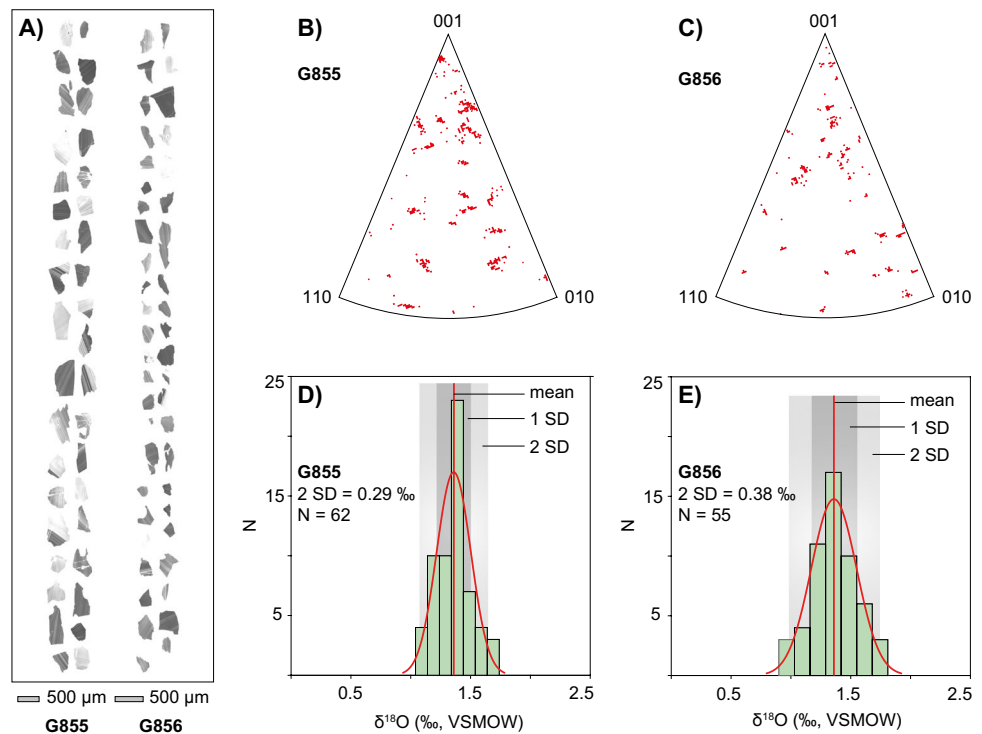
Our Yongde cassiterite (Figs. 1A and 2A–C) was from a gem dealer. The original mega-crystal had been cut to make jewelry, leaving an irregular fragment that was investigated here (Fig. 2A). The cassiterite was collected from a granite-related Sn(-W) mine/outcrop in Yalian town (N24° 11', E99° 36'), Yongde county, Yunnan province, but the exact sampling location is not known. The Yongde-Cst is transparent to semi-transparent with a milky gray color (Fig. 2A), and has a weight of ~30 g. The sample is reasonably clean with no fractures or cracks, except for the presence of wolframite inclusions in a limited area (~3 mm).

Cassiterite from six Chinese Sn(-W) deposits

The Xiaolonghe Sn deposit

The Xiaolonghe Sn deposit (N25° 27', E98° 26') is located in the Tengchong-Lianghe district, which is an important tin mineralization area in the Sanjiang Tethyan Metallogenic Domain of Southwest China. It comprises four mining sections from west to east, namely the Xiaolonghe, the Wandanshan, the Huangjiashan, and the Dasongpo. Mineralization is genetically associated with a biotite monzogranite that has porphyritic, medium- to coarse-grained, and fine-grained facies. The biotite monzogranite was emplaced at 71.4 ± 0.4 Ma as dated by LA-ICP-MS zircon U–Pb (Cao et al. 2016). Tin mineralization mainly developed as greisen and quartz veins in the contact zone between the biotite monzogranite and sedimentary wall rocks, and within the cupola of the granitic stock. The mineralization age ($71.6 \pm 2.4 - 73.9 \pm 2.0$ Ma) was defined by LA-ICP-MS cassiterite U–Pb dating (Chen et al. 2014). Fluid inclusion assemblages hosted in quartz, topaz, and cassiterite mostly are liquid-rich with a salinity of ~15 wt% NaCl equiv., and a homogenization temperature of 423–450 °C (Cui et al. 2019). Samples XLH, RD, and DSPK were collected from the Xiaolonghe, Huangjiashan, and Dasongpo mining sections, respectively.

Fig. 1 SIMS oxygen isotope composition and crystallographic orientation information of cassiterite fragments of the Yongde-Cst. **A** CL images of cassiterite fragments from the Yongde-Cst; fragments with sizes ranging from ~300 μm to ~1 mm were cast in two epoxy resin mounts (G855 and G856). **B** Inverse pole figure map of cassiterite fragments on mount G855; a stereographic triangle is used to represent the crystallographic orientation with respect to three major planes (i.e., 111, 100, 110). **C** Inverse pole figure map of cassiterite fragments on mount G856. **D** Histogram of SIMS $\delta^{18}\text{O}$ values of cassiterite fragments on mount G855. **E** Histogram of SIMS $\delta^{18}\text{O}$ values of cassiterite fragments on mount G856



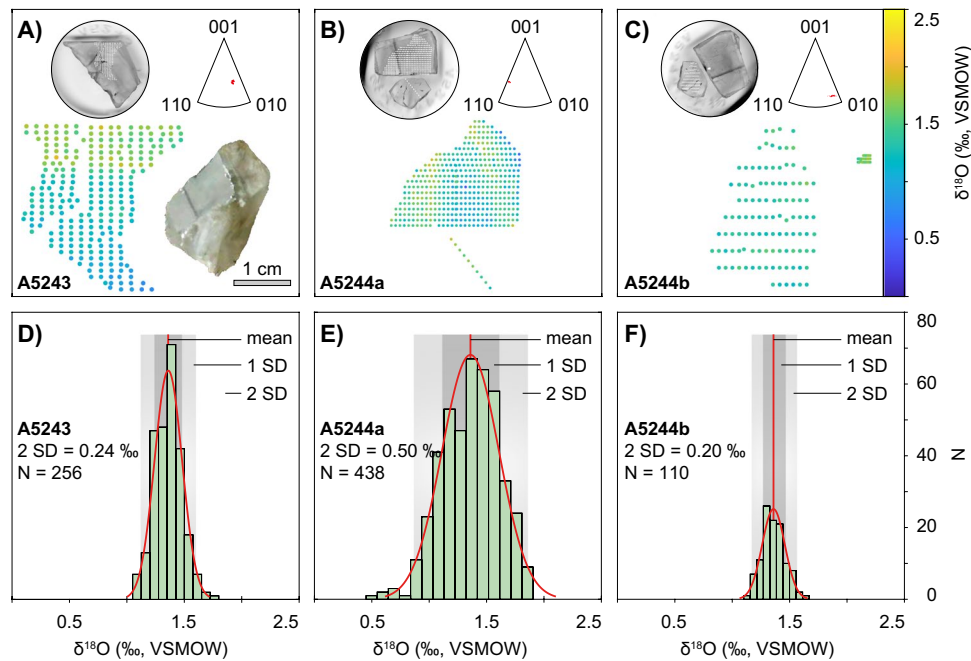


Fig. 2 SIMS $\delta^{18}\text{O}$ values of the Yongde-Cst. **A** Horizontal section of the Yongde-Cst cast in epoxy resin as mount A5243; pits of SIMS $\delta^{18}\text{O}$ analysis are illustrated with a color scheme to represent their measured $\delta^{18}\text{O}$ values; there is a gradual increase in measured $\delta^{18}\text{O}$ values along the Y axis, which indicates the presence of a position effect and has been corrected (Li et al. 2021); also presented is an inverse pole figure map of the studied cassiterite surface; an inserted photo at bottom right shows the Yongde-Cst studied here before cutting. **B** Vertical section (fragment on top) of the Yongde-Cst cast in epoxy resin as mount A5244; also shown are pits of SIMS $\delta^{18}\text{O}$ analysis and an inverse pole figure map of the exposed surface; a traverse was conducted across the horizontal section (big fragment in mount A5244) and the sharp end (small fragment in mount A5244) to assess

isotopic homogeneity of the two fragments; NIST610 glass was analyzed to monitor instrumental drift. **C** A small tip (the sharp end) of the Yongde-Cst cast in epoxy resin together with the vertical section as mount A5244; also shown are pits of SIMS $\delta^{18}\text{O}$ analysis and an inverse pole figure map of the exposed surface; A 900 * 200- μm area from the horizontal section was analyzed with a 100 * 100- μm grid to monitor instrumental drift. **D** Histogram of SIMS $\delta^{18}\text{O}$ values of the horizontal section of the Yongde-Cst after correcting the Y-coordinate-related position effect following Li et al. (2021). **E** Histogram of SIMS $\delta^{18}\text{O}$ values of the vertical section of the Yongde-Cst. **F** Histogram of SIMS $\delta^{18}\text{O}$ values of the small tip (the sharp end) of the Yongde-Cst

The Hehuaping Sn(-W) deposit

The Hehuaping Sn deposit (N25° 45', E113° 06') is located in southern Hunan province, Chinese Nanling Range. Tin mineralization is genetically associated with a hidden biotite granite pluton and granite porphyry dykes, which have emplacement ages of $157.1 \pm 0.8 - 154.9 \pm 0.5$ Ma, as defined by LA-ICP-MS zircon U–Pb dating (Zhang et al. 2015). The tin deposit mainly consists of skarn, porphyry, and greisen ores. Five main orebodies in the Hehuaping tin deposit were delineated. Number IV orebody is the largest and developed between dolomitic limestone of the Devonian Qiziqiao Formation and sandstone of the Tiaomajian Formation. It is related to a magnesian skarn system with a mineral assemblage of forsterite, spinel, diopside, tremolite, serpentine, talc, and phlogopite (Yao et al. 2014). The cassiterite-magnetite orebody in the proximal skarn is

3.4 km long. Cassiterite grains co-existing with magnetite are very small (< 100 μm). In the distal skarn, cassiterite-sulfide veins are common and crosscut the marble. The cassiterite has a relatively larger grain size (> 100 μm) in comparison to those from the proximal skarn. Four paragenetic stages of skarn and ore formation have been recognized: (I) prograde stage (spinel, forsterite, and diopside), (II) retrograde stage (serpentine, phlogopite, tremolite), (III) cassiterite-sulfide stage (cassiterite, magnetite, galena, sphalerite, pyrrhotite, pyrite, chalcopyrite, and arsenopyrite), and (IV) carbonate stage (siderite, rhodochrosite, calcite, and fluorite). Quartz and fluoride-hosted fluid inclusion assemblages (Yao et al. 2014) revealed that the major ore-forming fluids from stage III are characterized by low temperature (170 to 240 °C) and low salinity (1 to 6 wt% NaCl equiv.). Sample IV was collected from the no. IV orebody.

The Tongkeng Sn(-W) deposit

The Tongkeng Sn(-W) deposit (N24° 58', E107° 30') from Dachang Sn district is located in the Youjiang Basin, South China. The Tongkeng-Changpo Sn(-W) deposit is the largest Sn deposit in this district. It lies at the northeast limb of the Dachang anticline, and approximately 4 km southwest of the Longxianggai granitic pluton (Cai et al. 2007). The deposit is hosted in the Upper Devonian limestone and siliceous rocks, and comprises cassiterite-bearing veins and stockworks in the upper part and stratiform Sn-Zn-Pb ores in the lower part (Fu et al. 1991). LA-ICP-MS U-Pb dating of cassiterite from the Tongkeng orebody yielded a mineralization age of 91.6 ± 2.4 Ma (Guo et al. 2018b), which is consistent with the zircon U-Pb age ($96.6 \pm 2.5 - 93.9 \pm 0.9$ Ma) of the Longxianggai granitic pluton (Liang et al. 2011). Three mineralization stages have been identified based on the mineral association and crosscutting relationships (Fu et al. 1991; Cai et al. 2007), i.e., stage I with cassiterite-pyrite/pyrrhotite-tourmaline-quartz, stage II with cassiterite-sphalerite-sulfosalt-quartz, and stage III with calcite-quartz \pm sulfide \pm sulfosalt. Cassiterite mainly formed during stages I and II, and is light yellowish in color. Homogenization temperatures of quartz-hosted fluid inclusion assemblages from stages I, II, and III are 270–365 °C, 210–240 °C, and 140–190 °C, respectively (Cai et al. 2007). Sample TK was collected from a cassiterite vug in the Tongkeng deposit.

The Kafang Sn(-W) deposit

The Kafang Sn(-W) deposit (N23° 22', E103° 09') is in Gejiu Sn district. Located in the Youjiang Basin (Guo et al. 2018a), Gejiu is one of the largest tin district in the world. The Kafang Sn deposit is located in the southernmost part of the Gejiu ore district. Skarn type Cu-Sn ores mainly distribute at the contact between the Xinshan granite and carbonate. Stratiform Cu ores hosted by basalt and stratiform Cu-Sn ores hosted by carbonate also are well-developed in the mining area. Tin mineralization only is developed in the skarn type and stratiform orebodies hosted by carbonate (Cheng et al. 2012). Molybdenite from the skarn Cu-Sn ore yielded a Re-Os isochron age of 83.4 ± 2.1 Ma, which is coeval with the zircon U-Pb age (83.1 ± 0.4 Ma) of the Xinshan granite (Cheng et al. 2012). Homogenization temperatures of vapor-rich, vapor phase-moderate, and vapor phase-poor types of fluid inclusion assemblages hosted by quartz are 279.3–452.0 °C, 161.6–342.4 °C, and 105.2–227.8 °C, respectively (Cheng et al. 2012). Sample KF was collected from the skarn type Cu-Sn ore.

The Xishan Sn(-W) deposit

The Xishan Sn(-W) deposit (N22° 8', E111° 40') is located in the western part of the Yangchun basin. Tin orebodies of the Xishan Sn(-W) deposit mainly occur in quartz veins, greisen, and skarn (Cao et al. 2016). The quartz-vein type ore is the most important ore type in the mining area, which is mainly developed in the copula of the Xishan granitic pluton. Greisen mineralization lies in the copula of the Xishan pluton and consists mainly of quartz, muscovite, and topaz, with minor cassiterite and fluorite. Skarn mineralization is formed in the contact zone between the limestone and the Xishan pluton. Ore minerals are cassiterite and wolframite. LA-ICP-MS zircon U-Pb dating of the Xishan granitic pluton defines an emplacement age of $79.3 \pm 0.8 - 78.1 \pm 0.9$ Ma, which is consistent with the mineralization age of the Xishan Sn(-W) deposit, as constrained by molybdenite Re-Os isochron dating (79.4 ± 4.5 Ma) and LA-ICP-MS cassiterite U-Pb dating ($79.0 \pm 1.2 - 78.1 \pm 0.9$ Ma) for the cassiterite-quartz veins (Zhang et al. 2017). Sample XS was collected from a quartz vein in a quarry.

The Lailishan Sn(-W) deposit

The Lailishan Sn deposit (N24° 56', E98° 16') is located in the Tengchong-Lianghe district. The orebodies mainly developed as greisen lenses and cassiterite-sulfide veins in the contact zones between the granites and Carboniferous wall rocks, or the fractured zones surrounding the granitic intrusions. Cassiterite U-Pb and zircon U-Pb dating results show that the tin mineralization and granitic magmatism were broadly coeval at $50.0 \pm 2.7 - 47.4 \pm 2.0$ Ma (Chen et al. 2014). The tin mineralization process can be divided into three successive mineralization stages, and homogenization temperatures of cassiterite-hosted fluid inclusions from these stages are 216–337 °C, 116–199 °C, and 160–243 °C, respectively (Wang et al. 2020). Sample V109 was collected from the greisen orebody, whereas sample LLSK was from the cassiterite-sulfide veins in the breccia ore.

Analytical methods

Sample preparation

The sharp end of the Yongde-Cst was cut by a wire saw to create a flat surface for further sample preparation. After the sharp end had been removed, the fragment was sliced into two halves along its vertical section. One vertical section was further cut along its horizontal section into two pieces. The sharp end, uncut vertical section, and horizontal section were polished by using a 400-grit sandpaper and then were cast into epoxy resin as standard 25-mm mounts. The

vertical section was cast in mount A5243 (Fig. 2A), and the horizontal section and the sharp end were cast in A5244 (Fig. 2B). These mounts were firstly ground using 800-grit sandpapers, with further grinding by a 10- μm diamond paste using an automatic polisher. To remove scratches from the surface of the grains, the mounts were further polished by 0.5- μm and 0.25- μm diamond paste successively. Between each grinding and polishing step, the mounts were cleaned in ethanol using an ultrasonic cleaner for 20 s to remove polishing materials from previous steps. With careful grinding and polishing, the mounts are expected to have a very small topography with a relief of less than 3 μm , which is critical for high-quality SIMS oxygen isotope measurements (Tang et al. 2015).

The second horizontal section of the Yongde-Cst was crushed into aliquots with sizes ranging from 200 to 800 μm ; then ~ 40 aliquots were randomly chosen and mounted together with cassiterite grains from six Sn(-W) deposits as mounts G855 and G856 (Fig. 1A). About 100 mg of the crushed Yongde-Cst was ground to 200-mesh for oxygen isotope measurements by gas source isotope ratio mass spectrometry.

Cathodoluminescence imaging

Cathodoluminescence (CL) imaging was conducted at Nanjing Hongchuang Geological Exploration Technology Service Company. Images were collected on a Tescan MIRA3 LM instrument equipped with a CL detector. Before analysis, mounts were cleaned by ethanol using an ultrasonic cleaner. Once dried, the mounts were carbon-coated with a thickness of ~ 10 nm to improve electrical conductivity. For CL imaging, acceleration voltage and beam current during the course of study were 14 kV and 1.2 nA, respectively. The working distance between CL detector and sample surface was ~ 18.8 mm. Depending on grain size, magnification varied from 150 to 300. Each CL image was collected by an accumulation of 80 s.

Electron backscatter diffraction

Electron backscatter diffraction (EBSD) studies were performed using a ZEISS Crossbeam 540 scanning electron microscope (SEM) with an EBSD unit from Oxford Instruments at the Institute of Geology and Geophysics, Chinese Academy of Sciences. For better EBSD measurements, a chemical polishing step using colloidal silicon was applied after our standard metallographic polishing procedures described above.

Sample mounts were cleaned in deionized water using an ultrasonic cleaner. Once dried, we applied a ~ 10 -nm carbon coating on mount surface to improve its electrical conductivity. Using the same structure model of Carr et al. (2017) for

cassiterite, diffraction patterns of cassiterite were obtained using a beam voltage of 20 kV, a beam current of 1–2 nA, and a spot size diameter of 10 nm. Orientation information was collected pixel by pixel with a pixel spacing of 100 nm. Inverse pole figure maps (Figs. 1B–C and 2A–C) of the analyzed cassiterite grains were generated to illustrate the orientation of the cassiterite grains with respect to the major poles (111, 100, 110) of the stereographic triangle.

Secondary ion mass spectrometry

SIMS oxygen isotope analysis for all cassiterite samples was conducted at the Beijing Research Institute of Uranium Geology (BRIUG) on a CAMECA IMS 1280HR SIMS. An exception was the horizontal section of the Yongde-Cst in mount A5244, which was measured at the Institute of Geology and Geophysics, Chinese Academy of Sciences (IGGCAS) with a CAMECA IMS 1280 SIMS.

For mount A5243 and A5344, they were measured by SIMS with a 500 * 500 μm grid (Fig. 2A–B). There was a fracture in the middle of the grain in A5243 (Fig. 2A), which was generated during sample preparation, and that fractured area was avoided when selecting SIMS targets. For mount A5244 (Fig. 2B), a traverse was conducted across the horizontal section (big fragment in mount A5244) and the sharp end (small fragment in mount A5244) to assess isotopic homogeneity of the two fragments. To monitor instrumental drift during the measurements of mount A5244 at IGGCAS, NIST610 glass, which is expected to have a homogenous oxygen isotope composition, was measured twice after each 10 measurements of the Yongde-Cst. Please note that a few aliquots of NIST610 have very different oxygen isotope composition. At BRIUG, to monitor instrumental drift and to evaluate potential isotopic heterogeneity between the horizontal section (big fragment in mount A5244) and the sharp end (small fragment in mount A5244), a 900 * 200- μm area from the horizontal section was analyzed with a 100 * 100- μm grid (Fig. 2C). The selected area was analyzed twice after each 10 measurements of the sharp end of the Yongde-Cst.

Instrumental conditions, analytical procedure, and data reduction processes are the same in both laboratories after modification from previous studies (Li et al. 2009; Tang et al. 2020; Li et al. 2021). Prior to analysis, mounts were cleaned by ethanol using an ultrasonic cleaner. Once dried, they were coated with a ~ 50 -nm gold film to improve electrical conductivity. A normal incident electron flood gun was used to compensate for electrical charging. We used ~ 2 nA Cs^+ ions with an accelerating energy of +10 kV as the primary beam to liberate $^{16}\text{O}^-$ and $^{18}\text{O}^-$ from the samples. An accelerating voltage for secondary ions was set to -10 kV. The primary beam was focused in Gaussian mode, and the analytical spot as a square had a size of $10 * 15 \mu\text{m}^2$.

An energy window of 50 eV was used at the low energy band, and the mass resolution defined as $M/\Delta M$ at 50% peak height was set to 3000. A nuclear magnetic resonance controller was applied at IGGCAS, but not at BRIUG. Prior to analysis, a 60-s sputtering under raster mode was applied to remove the gold coating, and to clean the sample surface. After 60 s of automatic beam centering, oxygen isotope measurements were achieved through a 96-s integration, which were divided into 20 cycles, and each cycle contained 4-s isotope measurement plus 0.8-s waiting time. Each spot-measurement took 216 s. Oxygen isotopes (^{16}O and ^{18}O) were measured simultaneously on two Faraday cups equipped with 10^{10} and 10^{11} Ω resistors, respectively, and a $^{16}\text{O}^-$ intensity of $\sim 3.5 \times 10^9$ counts per second (cps) was obtained in our routine measurements. Instrumental uncertainty from counting statistics for individual analysis (i.e., internal precision) was generally better than 0.2‰ (2σ).

Measured $^{18}\text{O}/^{16}\text{O}$ ratios are converted to raw $\delta^{18}\text{O}$ values ($\delta^{18}\text{O}_{\text{measured}}$) through normalizing the measured $^{18}\text{O}/^{16}\text{O}$ ratios to that of the Vienna Standard Mean Ocean Water (0.0020052, VSMOW) as outlined in Eq. 1.

$$\delta^{18}\text{O}_{\text{measured}}(\text{inpermil}) = ({}^{18}\text{O}/{}^{16}\text{O}_{\text{measured}} \div 0.0020052 - 1) \times 1000 \quad (1)$$

For mount 5243 and mount 5244, our primary concern is their homogeneity in terms of oxygen isotope composition. Hence, only the measured $\delta^{18}\text{O}$ values are needed (see the “Discussion” session for further details on this topic). This is also the case for the Yongde-Cst in mount G855 and mount G856 when evaluating crystallographic orientation effects.

For cassiterite samples from six Sn(-W) deposits, correction of instrumental mass fractionation is essential to yield true $\delta^{18}\text{O}$ values relative to the VSMOW scale. This is achieved through analyzing the Yongde-Cst between samples, which has been developed as a matrix-match reference material in this study (see below for discussion). The IMF is quantified through replicated analysis of the Yongde-Cst following Eq. 2.

$$\text{IMF} = \delta^{18}\text{O}_{\text{measured value of RM}} - \delta^{18}\text{O}_{\text{true value of RM}} \quad (2)$$

The true $\delta^{18}\text{O}$ value of our Yongde-Cst relative to the VSMOW scale has been defined by gas source isotope ratio mass spectrometry (see below for discussion). Once IMF has been obtained, $\delta^{18}\text{O}$ values of cassiterite samples are calculated following Eq. 3.

$$\delta^{18}\text{O}_{\text{sample}}(\text{VSMOW}) = \delta^{18}\text{O}_{\text{measured value of sample}} - \text{IMF} \quad (3)$$

Gas source isotope ratio mass spectrometry

The oxygen isotope composition of the Yongde-Cst was obtained by the furnace fluorination method (Feng et al. 2020)

at the Institute of Geology and Geophysics, Chinese Academy of Sciences. Chinese national reference material GBW04409 (quartz) was analyzed during the course of study for quality control purpose, and 5 analyses in the same period yield an average of $11.10 \pm 0.09\text{‰}$ (2 SD, VSMOW). Samples were fluorinated in a nickel reaction vessel, and each analysis consumed about 6 mg of material. Samples were loaded under a positive pressure of pure nitrogen gas to prevent adsorption of atmospheric moisture in the nickel reaction vessel. After the initial overnight pumping and a 10-min room-temperature fluorination with BrF_5 , the vessel was evacuated and charged again with an aliquot of BrF_5 . The nickel reaction vessel was heated to 750 °C with a resistance furnace for 4 h. Generated gases were purified through a series of cryogenic traps which were chilled by liquid nitrogen. The purified oxygen gas was analyzed on a viscous-flow mass spectrometer of Finnigan MAT252.

First-principles calculations

We obtained the equilibrium oxygen isotope fractionation between cassiterite and quartz using first-principles calculations based on the density functional theory. The equilibrium isotope fractionation factor of element X between two phases A and B, α_{A-B} , is the ratio of their isotope ratios in these two phases. According to the Bigeleisen-Mayer theory (Bigeleisen and Mayer 1947; Urey 1947), the isotope fractionation factor between the phase A and an ideal gas of X atoms is the reduced partition function ratio β_A of the element X. Within the harmonic approximation, the β_A can be expressed as:

$$\beta_A = \frac{Q_h}{Q_l} = \prod_i^{3N} \frac{u_{ih}}{u_{il}} \frac{e^{-\frac{1}{2}u_{ih}}}{1 - e^{-u_{ih}}} \frac{1 - e^{-u_{il}}}{e^{-\frac{1}{2}u_{il}}} \quad (4)$$

where Q is the vibrational partition function, and indexes h and l refer to the heavy and light isotope, respectively. The running index i refers to the vibrational frequency mode, and N is the number of atoms in the unit cell. Parameter u_{ih} or u_{il} is defined as:

$$u_{ih \text{ or } il} = h\omega_{ih \text{ or } il} / k_B T \quad (5)$$

where h and k_B are the Planck and Boltzmann constants, respectively. T is temperature in Kelvin, and $\omega_{ih \text{ or } il}$ is the vibrational frequency of the i^{th} mode. Following Richet et al. (1977), the equilibrium isotope fractionation between two phases A and B can be rewritten in per mil as:

$$\Delta_{A-B} = 1000 \ln \alpha_{A-B} = 1000 \ln \beta_A - 1000 \ln \beta_B \quad (6)$$

The calculation processes in this study are similar to those in our previous work (Huang et al. 2013; Wang et al. 2017). We performed all calculations using an open-source software “Quantum Espresso” based on the DFT, plane wave, and pseudopotential (Giannozzi et al.

2009). Local density approximation (LDA) was adopted for the exchange correlation functional (Perdew and Zunger 1981). The cutoff for plane-wave energy is 70 Ry. The pseudopotentials for oxygen and silicon were generated by the method of Troullier and Martins (1991) with a configuration of $2s^2 2p^4$ and a cutoff radius of 1.45 Bohr for oxygen and a configuration of $3s^2 3p^4 3d^0$ and a cutoff radius of 1.47 Bohr for silicon. The tin pseudopotential, `sn_lda_v1.4.uspp.F.UPF`, is an ultrasoft type generated using Vanderbilt method (Vanderbilt 1990), which is available in the online Quantum Espresso pseudopotential library (<http://www.quantum-espresso.org/pseudopotentials/>). Brillouin zone integrations over electronic states were performed with a $12 \times 12 \times 12$ k-point grid for quartz and a $10 \times 10 \times 14$ k-point grid for cassiterite. The crystal structures of quartz and cassiterite were optimized using variable cell shape molecular dynamics (Wentzcovitch 1991) and the residual forces converge within 10^{-4} Ry/Bohr. Their dynamical matrices were calculated on a regular q mesh of $2 \times 2 \times 2$ for quartz and $3 \times 3 \times 4$ for cassiterite using the density-functional perturbation theory and then interpolated on a dense q mesh to obtain the vibrational properties.

Oxygen isotope fractionation between cassiterite and water

Since the oxygen isotope fractionation between quartz and water has been well-established both experimentally and theoretically (Sharp et al. 2016 and references therein), oxygen isotope fractionation between cassiterite and water was obtained through using quartz as a bridge mineral. Specifically, with $1000 \ln \alpha$ of cassiterite and quartz being calculated from density functional theory method, we used $1000 \ln \alpha$ of quartz and water from Sharp et al. (2016) to calculate $1000 \ln \alpha$ of cassiterite and quartz using Eq. 7,

$$1000 \ln \alpha_{\text{cassiterite-water}} = 1000 \ln \alpha_{\text{quartz-water}} - 1000 \ln \alpha_{\text{quartz-cassiterite}} \quad (7)$$

A similar approach was utilized to calculate $1000 \ln \alpha$ of zircon and water, in which case $1000 \ln \alpha$ of zircon and quartz from Valley (2003) was used.

Results

Crystallographic orientation information

Crystallographic orientation information for the crushed aliquots of the Yongde-Cst in mounts G855 and G856 (Fig. 1A) was obtained by electron backscatter diffraction. The results are illustrated as inverse pole figures in Fig. 1B–C. As shown,

the aliquots cast in mount G855 and G856 cover a variety of orientations as defined by three major crystallographic planes (i.e., 001, 110, 101). This was expected since the crushed aliquots were randomly cast during sample preparation. These aliquots were further measured by SIMS, and measured $\delta^{18}\text{O}$ values (i.e., raw data without IMF corrections) from both mounts show limited variation. For mount G855, measured $\delta^{18}\text{O}$ values define a Gaussian distribution with two standard deviations of 0.29‰ (2 SD, $n=62$, Fig. 1D); for mount G856, 55 analyses define a Gaussian distribution with two standard deviations of 0.38‰ (2 SD, Fig. 1E).

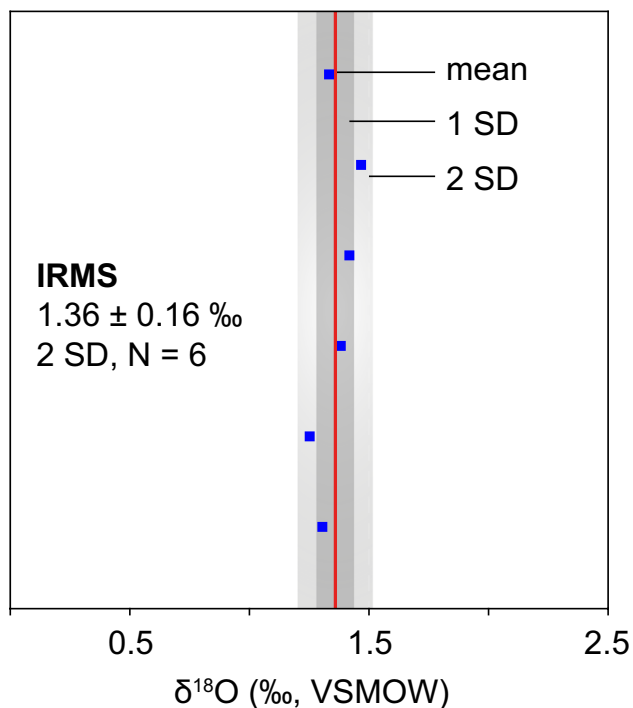
SIMS oxygen isotope of the Yongde-Cst

All SIMS measurements of cassiterite oxygen isotope composition are presented in Table S1 in the Supplementary information. For the vertical section of the Yongde-Cst in mount A5243 (Fig. 2A), the exposed sample surface has a uniform crystallographic orientation close to plane 010. In total, 256 analyses (mount A5243) were conducted continually for 19.7 h at BRIUG, and measured $\delta^{18}\text{O}$ values define a distribution close to Gaussian with two standard deviations of 0.54‰ (2 SD, $n=256$). The measured $\delta^{18}\text{O}$ values show a pronounced correlation with their Y-coordinates (Fig. 2A) with a R^2 of 0.8 (Table S1 in the Supplementary information). A similar phenomenon has been investigated in detail during apatite oxygen isotope analysis (Li et al. 2021), and this position effect has been attributed to the presence of a slope on sample surface or imperfect holder conductivity along the Y direction, which leads to an imperfect centering of the trajectory of secondary ions. In this regard, a correction was applied for this Y-coordinate-related position effect following Li et al. (2021), and the corrected $\delta^{18}\text{O}$ values yield two standard deviations of 0.24‰ ($n=256$, Fig. 2D).

For the horizontal section of the Yongde-Cst in mount A5244, the exposed sample surface also shows a uniform crystallographic orientation close to plane 110 (Fig. 2B). The analytical time for the traverse and the horizontal sections were 2.5 h and 32.75 h, respectively. In total, 438 analyses were conducted for the Yongde-Cst in mount A5244 at IGGCAS, and measured $\delta^{18}\text{O}$ values define a normal distribution with two standard deviations of 0.50‰ (2 SD, $n=438$, Fig. 2E), and NIST610 yields two standard deviations of 0.35‰ (2 SD, $n=80$). All analyses of NIST610 showed no time-dependent drift, and this demonstrates that the instrument was stable at the 0.35‰ level during the course of study; hence, no time drift correction was applied. These measurements also show no dependence on sample coordinates and instrumental tuning parameters (e.g., DTFA and DTCA, Table S1).

Table 1 Oxygen isotope composition of the Yongde-Cst determined by gas source isotope ratio mass spectrometry

Number	$\delta^{18}\text{O}$ (‰, VSMOW)
1	1.31
2	1.25
3	1.38
4	1.42
5	1.47
6	1.33
Average	1.36
2 SD	0.16

**Fig. 3** Oxygen isotope composition of the Yongde-Cst determined by gas source isotope ratio mass spectrometry

For the sharp end of the Yongde-Cst, the exposed surface has a uniform crystallographic orientation close to plane 010 (Fig. 2C). The analysis lasted 8.5 h, and 110 measurements from the sharp end of the Yongde-Cst define a normal distribution with two standard deviations of 0.20‰ (2 SD, $n = 110$, Fig. 2F).

IRMS oxygen isotope measurements of the Yongde-Cst

Six measurements of the Yongde-Cst by gas source isotope ratio mass spectrometry at IGGCAS are listed in Table 1. The results show limited variations in $\delta^{18}\text{O}$ values between

1.25 and 1.47‰ and give an average of 1.36 ± 0.16 ‰ (VSMOW, 2 SD, $n = 6$, Fig. 3).

Oxygen isotope fractionation between quartz and cassiterite

Calculated oxygen isotope fractionation at 50–850 °C for quartz and cassiterite is given by Eq. 8 as follows:

$$1000 \ln \alpha_{\text{quartz-cassiterite}} = 1.259 \times 10^6 / T^2 + 8.15 \times 10^3 / T - 4.72 \quad (8)$$

where T is the temperature in Kelvin. The equation is plotted in Fig. 4A–B, with $1000 \ln \alpha$ from previous computational and experimental studies being graphically illustrated as well (Zheng 1991; Zhang et al. 1994; Hu et al. 2005; Polyakov et al. 2005). Our calculation agrees remarkably well with recent computational and experimental studies; this convergency most likely results from advances in computing and improvements in experimental studies over the last decades. Using the well-established $1000 \ln \alpha$ of quartz and water (Fig. 4D) from Sharp et al. (2016), the oxygen isotope fractionation between cassiterite and water (Fig. 4C) is outlined in Eq. 9 as follows,

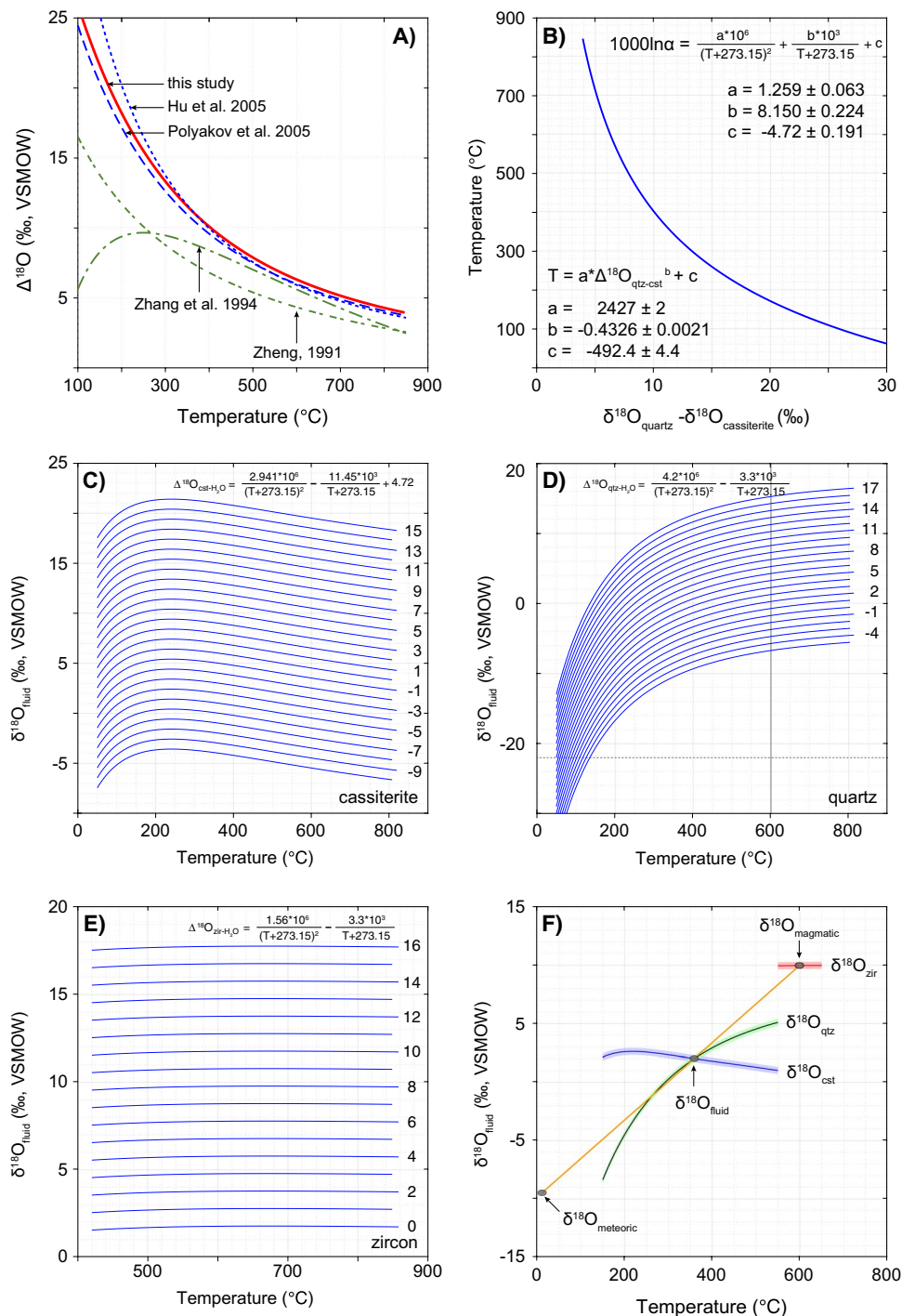
$$1000 \ln \alpha_{\text{cassiterite-water}} = 2.941 \times 10^6 / T^2 - 11.45 \times 10^3 / T + 4.72 \quad (9)$$

We also derived oxygen isotope fractionation between zircon and water (Fig. 4E) using $1000 \ln \alpha$ of quartz-zircon and quartz-water from Valley (2003) and Sharp et al. (2016) respectively, and the $1000 \ln \alpha$ of zircon-water is described by equation of $1.56 \times 10^6 / T^2 - 3.3 \times 10^3 / T$ (T is temperature in Kelvin). We note here that $1000 \ln \alpha$ of quartz-zircon reported in literature have considerable variations, and our preferred calibration from Valley (2003) is broadly consistent with those estimated from natural systems and a recent experimental study (Trail et al. 2009 and references therein).

When using $1000 \ln \alpha$ of mineral–water (i.e., cassiterite–water, quartz–water and zircon–water) to derive oxygen isotope composition of fluids, uncertainties from both oxygen isotope measurements and temperature estimates have been propagated using a Monte Carlo approach (Li et al. 2019).

SIMS oxygen isotope analyses of cassiterite from Sn(-W) deposits

Nine cassiterite samples from six Sn(-W) deposits were measured by SIMS with an aim to constrain the oxygen isotope composition of ore-forming fluids. Representative CL images of these samples are shown in Fig. 5A, with SIMS $\delta^{18}\text{O}$ data being illustrated in Fig. 5B. In general, the studied samples show well-developed oscillatory zonation in CL images. It should be noted that a few samples show alteration features with primary zonation being truncated by CL-bright bands.



To investigate the oxygen isotope composition of cassiterite samples with alteration, one sample (DSPK) showing a low degree of alteration was selected along with two fresh samples (XLH, RD) from the Xiaolonghe Sn(-W) deposit, Yunnan for SIMS analysis. Three samples yield similar $\delta^{18}\text{O}$ values with variations between 1.86 and 4.13‰, and average $\delta^{18}\text{O}$ values for XLH, RD, and DSPK are $3.56 \pm 0.51\text{‰}$ (2 SD, $n = 13$), $2.81 \pm 0.73\text{‰}$ (2 SD, $n = 21$), and $3.25 \pm 1.17\text{‰}$ (2 SD,

$n = 31$), respectively. The degree of alteration has had no measurable matrix effects on the oxygen isotope composition.

Samples from the Huhuaping Sn(-W) deposit, Hunan province (IV); the Dachang Sn(-W) deposit, Guangxi province (TK); the Kafang Sn(-W) deposit, Yunnan province (KF); and the Xishan Sn(-W) deposit, Guangdong province (XS) all have well-developed oscillatory zonation with no sign of alteration. Samples from the same

Fig. 4 Oxygen isotope exchange in the cassiterite, quartz, zircon, and water systems. **A** Oxygen isotope fractionation between quartz and cassiterite as a function of temperature from previous studies (Zheng 1991; Zhang et al. 1994; Hu et al. 2005; Polyakov et al. 2005) and recalculated in this study. **B** A sensitive response between $1000 \ln \alpha$ of quartz-cassiterite and temperature, as quantified by $1.259 \times 10^6/T^2 + 8.15 \times 10^3/T - 4.72$ (T is temperature in Kelvin), makes quartz-cassiterite very promising for oxygen isotope thermometry. **C** Oxygen isotope fractionation of cassiterite-water as a function of temperature, as quantified by the equation of $2.941 \times 10^6/T^2 - 11.45 \times 10^3/T + 4.72$, where T is temperature in Kelvin; it shows a weak and negative response to temperature; such a weak temperature dependence makes it possible to predict the $\delta^{18}\text{O}$ values of ore-forming fluids without robust prior knowledge of the mineralization temperatures. **D** Oxygen isotope fractionation of quartz-water as a function of temperature, and the corresponding equation is $4.2 \times 10^6/T^2 - 3.3 \times 10^3/T$, where T is temperature in Kelvin; it shows a sensitive response to temperature, and the positive response gets more sensitive at low-temperature regions, which highlights the importance of getting accurate temperature estimates when calculating $\delta^{18}\text{O}$ values of fluids from quartz. **E** Oxygen isotope fractionation of zircon-water as a function of temperature, and the corresponding equation is $1.56 \times 10^6/T^2 - 3.3 \times 10^3/T$, where T is temperature in Kelvin. **F** A conceptual model to derive the nature of ore-forming fluids in magmatic-hydrothermal systems from an oxygen isotope perspective; using a binary mixing model, oxygen isotope composition of magmatic water, ore-forming fluids, and meteoric water as well as temperatures of ore formation all can be constrained with the $\delta^{18}\text{O}$ values of zircon, quartz, and cassiterite as inputs. In this model, temperature of the mixture (i.e., hydrothermal fluids) can be calculated using the equation of $T_{\text{hydrothermal}} = T_{\text{magmatic}} \times p + T_{\text{meteoric}} \times (1-p)$, where p is the proportional contribution of magmatic water. Similarly, oxygen isotope composition of the hydrothermal fluid also can be estimated as $\delta^{18}\text{O}_{\text{hydrothermal}} = \delta^{18}\text{O}_{\text{magmatic}} \times p + \delta^{18}\text{O}_{\text{meteoric}} \times (1-p)$. Assuming primary magmatic fluids have a temperature of ~ 600 °C, its oxygen isotope composition can be calculated from equilibrium isotope fractionation of zircon-water. Both temperature and oxygen isotope composition of hydrothermal fluids can be obtained using a quartz-cassiterite thermometer (or fluid inclusion studies) and $1000 \ln \alpha$ of cassiterite-water, respectively (see text for details)

deposit show very limited variations in terms of $\delta^{18}\text{O}$ values, but vary significantly between deposits. Average $\delta^{18}\text{O}$ values for IV, TK, KF, and XS are $3.27 \pm 0.42\text{‰}$ (2 SD, $n = 32$), $4.79 \pm 0.75\text{‰}$ (2 SD, $n = 38$), $1.46 \pm 1.06\text{‰}$ (2 SD, $n = 18$), and $3.02 \pm 0.58\text{‰}$ (2 SD, $n = 20$), respectively.

Two samples from the Lailishan Sn(-W) deposit, Yunnan province, show the highest degree of alteration among samples investigated in this study, though remnants of primary oscillatory zonation still can be seen from CL images (Fig. 5A). Measured $\delta^{18}\text{O}$ values show considerable variations for both samples, which range from -3.07 to 2.86‰ . Average $\delta^{18}\text{O}$ values for V109 and LLSK are $-0.20 \pm 3.04\text{‰}$ (2 SD, $n = 27$) and $1.42 \pm 2.72\text{‰}$ (2 SD, $n = 21$), respectively. Notably, zones with alteration consistently give low $\delta^{18}\text{O}$ values (peak at $-1.3 \pm 0.4\text{‰}$), while zones with the least alteration have $\delta^{18}\text{O}$ values of $1.6 \pm 0.4\text{‰}$ (Fig. 5B).

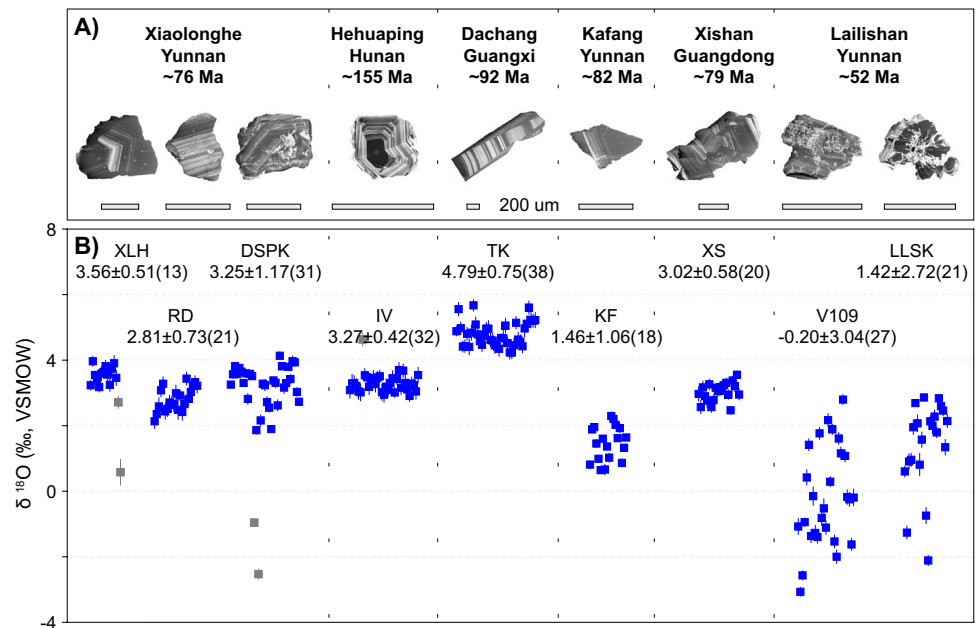
Discussion

No crystallographic orientation effects on SIMS cassiterite oxygen isotope analyses

Crystallographic orientation effects pose serious challenges for robust SIMS isotope analysis, particularly of oxide minerals (Huberty et al. 2010; Taylor et al. 2012). Our oxygen isotope analysis of the Yongde-Cst has sampled a range of crystallographic orientations with almost all three major planes being covered (Fig. 1B–C), but variations in $\delta^{18}\text{O}$ values are minimal (0.29 – 0.38‰ , Fig. 1D–E). A previous attempt on cassiterite oxygen isotope analysis via SHRIMP SI revealed $\sim 2\text{‰}$ variation for grains with variable crystallographic orientations (Carr et al. 2017), although in that case sample heterogeneity was a possible problem. Our results from both sessions are at the same level with current analytical precision (e.g., ~ 0.2 – 0.3‰); hence, the crystallographic orientation effects for CAMECA IMS 1280 SIMS cassiterite oxygen isotope analysis are negligible with the current analytical precision. Since SHRIMP SI and CAMECA 1280 SIMS have very different instrumental designs, which have been shown to pose significantly and contrastingly different effects on the magnitude of matrix effect during oxygen isotope analysis of olivine (Isa et al. 2017; Scicchitano et al. 2018), it is reasonable to speculate that SHRIMP SI may also behave differently from CAMECA SIMS in crystallographic orientation effects. Carr et al. (2017) has documented an intra-grain variation of $\sim 2\text{‰}$ with a single crystallographic orientation in their SHRIMP SI analysis, which is the same with variation of analysis from a range of crystallographic orientations. As such, it is clear that crystallographic orientation effect does not add additional variations beyond sample heterogeneity in their study. Along with our new observations, we conclude that the crystallographic orientation effect is probably negligible for ion microprobe (i.e., CAMECA 1280 SIMS and SHRIMP SI) cassiterite oxygen isotope analysis. If indeed present, it should not be larger than current analytical precision (~ 0.2 – 0.3‰). This will pave the way for robust cassiterite oxygen isotope analysis and facilitate geological applications in the study of ore-forming processes.

It is interesting to note that rutile shows significant crystallographic orientation effects during SIMS oxygen isotope analysis (Schmitt and Zack 2012; Taylor et al. 2012; Shulaker et al. 2015). Rutile is an isostructural mineral with cassiterite, so the contrasting behaviors between cassiterite and rutile make it unlikely that there is a link between crystallographic orientation effects and mineral structures. A plausible hypothesis to explain this contrasting behavior for isostructural minerals comes from the bonding element (e.g., Sn vs Ti) with oxygen, which could have an impact on

Fig. 5 SIMS oxygen isotope analyses of cassiterite from six Sn(-W) deposits. **A** CL images of representative cassiterite grains from the studied Sn(-W) deposits. Note that most cassiterite grains show well-developed oscillatory zonation, while a few samples have alteration features with primary zonation being truncated by bright bands. **B** $\delta^{18}\text{O}$ values of cassiterite from the studied Sn(-W) deposits. Samples with no sign of alteration show limited variation in terms of $\delta^{18}\text{O}$ values, while samples with a high degree of alteration show considerable variation in $\delta^{18}\text{O}$ values. Data are presented as $X \pm Y(N)$, where X, Y and N are mean, 2 SD and number of analyses, respectively



focusing secondary ions as suggested previously (Huberty et al. 2010). Further investigation of possible mechanisms controlling crystallographic orientation effects is critical for SIMS analysis, but it is beyond the scope of this study and not discussed further.

The Yongde-Cst as a reference material for SIMS oxygen isotope analysis

Using matrix-matched reference materials to correct instrumental mass fractionation is fundamental for accurate SIMS isotope analysis. For the developments of oxygen isotope reference materials for microanalysis, a main concern is its isotopic homogeneity. Our evaluation on the vertical and horizontal sections as well as the sharp end using a grid approach (Fig. 2A–C) revealed variations in $\delta^{18}\text{O}$ values of 0.24‰, 0.50‰, and 0.20‰, respectively (Fig. 2D–F).

Both the selected 900 * 200- μm area from the horizontal section (Fig. 2C and F) and NIST610 analyzed for monitoring instrumental drift show very limited variations (2 SD = 0.30‰, $n = 26$; 2 SD = 0.35‰, $n = 80$) in an extended period (8.5 h and 32.75 h) with no time dependence. These results suggest that instrumental drift in this study has been limited to less than 0.3‰ for a few tens of hours. As such, variations of 0.24‰ (2SD, $n = 256$) and 0.20‰ (2SD, $n = 110$) in $\delta^{18}\text{O}$ values observed here for the vertical section and the sharp end respectively are similar to instrumental noise, and we consider that they are homogeneous in terms of oxygen isotope composition. However, variations in $\delta^{18}\text{O}$ values of the horizontal section (2 SD = 0.50‰, $n = 438$) are apparently large for a homogenous sample. Other sources that may account for this extra scatter are position effect and topography effect. It is well-established that SIMS isotope

analyses are subject to position effects (Kita et al. 2009; Peres et al. 2013), but no correlation has been observed between measured $\delta^{18}\text{O}$ values of the horizontal section and their position and renders position effect as an unlikely cause for the extra scatter. Hence, the observed variations of the horizontal section (0.50‰) are more likely arising from topography effects. This has been further supported by limited variation (0.29–0.38‰) in $\delta^{18}\text{O}$ values for crushed fragments in mounts G855 and G856 (Fig. 1D–E). To summarize, our SIMS analysis demonstrates that the Yongde-Cst has a homogeneous oxygen isotope composition at the micrometer level, and it meets the criteria as a reference material for microanalysis. Recommended $\delta^{18}\text{O}$ values of the Yongde-Cst relative to VSMOW scale have been defined by GS-IRMS as $1.36 \pm 0.16\text{‰}$ (Fig. 3, 2 SD, $n = 6$). Yongde-Cst is the first cassiterite reference material for oxygen isotope microanalysis, and it is available to the scientific community immediately via the corresponding author upon reasonable request.

Cassiterite as a robust oxygen isotope record of ore-forming fluids

A diagnostic feature of the oxygen isotope fractionation between cassiterite and water is its insensitivity to temperature. The calculated $\delta^{18}\text{O}$ values of fluids only change by < 3‰ over a wide temperature range (200–800 °C, Fig. 4C). This feature is very different from that of quartz-water, which changes by 11‰ (Fig. 4D) over the same temperature range (Sharp et al. 2016 and references therein). The oxygen isotope composition of ore-forming fluids can be used to decipher fluid sources and to evaluate evolutionary processes during ore formation, and minerals

precipitated from these fluids are primary targets for deriving this information. However, calculating $\delta^{18}\text{O}$ values of fluids from $\delta^{18}\text{O}$ values of minerals requires knowledge of the temperature of isotope equilibrium between mineral and fluids. Independent temperature constraints for ore-forming fluids largely come from fluid inclusion studies. Obtaining temperatures from fluid inclusion studies is time-consuming, and getting accurate and precise estimates has been shown to be challenging, even for experienced researchers (Bodnar et al. 2014; Chi et al. 2021). Large uncertainties in temperature estimates could be very problematic when quartz, the most explored mineral in ore-forming fluid studies, has been studied to derive $\delta^{18}\text{O}$ values of fluids. For example, a variation of 100 °C in temperature estimates will add an uncertainty of 2.5‰ to the calculated $\delta^{18}\text{O}$ values of co-existing fluids from quartz (Fig. 4D). An insensitivity between oxygen isotope fractionation and temperature for the cassiterite-water system (Fig. 4C), on the other hand, loosens the requirements for robust temperature constraints. As discussed above, over a wide range of reasonable temperatures (150 to 600 °C) of cassiterite crystallization (Wood and Samson 2000), calculated $\delta^{18}\text{O}$ values of fluids change only by 1.68‰, or a decrease of less than 0.57‰ when temperature increases 100 °C (Fig. 4C). Hence, for situations where robust temperature constraints are difficult to obtain, a rough estimate in temperature does not include significant uncertainties in the calculated $\delta^{18}\text{O}$ values of fluids in cassiterite-water systems. An additional advantage in obtaining $\delta^{18}\text{O}$ of fluids from cassiterite over quartz is that cassiterite is a direct repository crystallized from metalliferous fluids, rather than assuming its precipitation from the same aliquots of metalliferous fluids when gangue minerals such as quartz are studied.

Quartz-cassiterite as an oxygen isotope geothermometer

Over a reasonable temperature range (150 to 600 °C) during Sn(-W) mineralization (Wood and Samson 2000), 1000 ln α of quartz and cassiterite show a strong dependence on temperature (Fig. 4A), which shows a sharp decrease of ~15‰ when temperature increases from 150 to 600 °C (Fig. 4B). Since quartz is the most abundant gangue minerals in Sn(-W) deposits, and its co-precipitation with cassiterite is not uncommon, this makes quartz-cassiterite a very promising oxygen isotope thermometer. The theoretical calibration of quartz-cassiterite oxygen isotope thermometer is described by the equation of T (°C) = $2427 \times (\delta^{18}\text{O}_{\text{qtz}} - \delta^{18}\text{O}_{\text{cst}})^{-0.4326} - 492.4$ (Fig. 4B). Current analytical precision for SIMS cassiterite and quartz oxygen isotope measurements is ~0.2–0.3‰; this corresponds to an uncertainty of 10 °C for temperature estimates from the analytical side. We have laid a firm ground for the application of quartz-cassiterite

geothermometry; both data from natural samples and experimental work are required to validate and to further calibrate our theoretical calibration.

The binary mixing model in magmatic-hydrothermal systems

Most Sn(-W) deposits are associated with granites, with ore-forming fluids being magmatic in origin, and then experienced variable degrees of mixing with meteoric water during ore precipitation (Legros et al. 2019; Harlaux et al. 2021). In addition to constraining temperatures of ore formation, estimating the proportion of meteoric water fluxing is also important to trace fluid evolutionary processes, and to decipher its role in metal deposition. This requires knowledge of the $\delta^{18}\text{O}$ values of meteoric water, but which is unknown in most cases, and in practice, an assumed value has been used.

For these systems, a binary mixing model can be used to quantify the proportional contribution of magmatic fluid and meteoric water (Fig. 4F). At the first order, the temperature of the mixture (i.e., hydrothermal fluids) can be calculated from the binary mixing model using equation of $T_{\text{hydrothermal}} = T_{\text{magmatic}} \times p + T_{\text{meteoric}} \times (1-p)$, where p is the proportional contribution of magmatic water. Oxygen isotope composition of the hydrothermal fluid also can be estimated following the binary mixing model in a similar fashion using equation of $\delta^{18}\text{O}_{\text{hydrothermal}} = \delta^{18}\text{O}_{\text{magmatic}} \times p + \delta^{18}\text{O}_{\text{meteoric}} \times (1-p)$. It is reasonable to assume that the temperature of primary magmatic fluids is approaching or slightly lower than the solidus of granitic magma (e.g., ~650 °C), and the $\delta^{18}\text{O}$ values of primary magmatic fluids also can be estimated with confidence from equilibrium zircon-water oxygen isotope fractionation (Fig. 4E). With temperatures of hydrothermal fluids being estimated from the quartz-cassiterite oxygen isotope thermometer, or independent fluid inclusions studies, $\delta^{18}\text{O}$ values of ore-forming fluids could be calculated from $\delta^{18}\text{O}$ values of cassiterite. To this end, a unique solution for the $\delta^{18}\text{O}$ values of meteoric water can be obtained following the binary mixing model. Hence, proportional contributions of magmatic fluids and meteoric water also can be calculated. Principles of this binary mixing model have been illustrated in Fig. 4F. The beauty of this method is that only $\delta^{18}\text{O}$ values of zircon, cassiterite, and quartz are needed, and the outcomes (e.g., ore-forming temperatures) could be validated by fluid inclusion studies. We also would like to emphasize here that the predicted $\delta^{18}\text{O}$ values of meteoric water most likely represent the $\delta^{18}\text{O}$ values of meteoric water experienced water–rock interaction, which may lead to significantly overestimated values. To decode the $\delta^{18}\text{O}$ values of primary meteoric water, it is critical to use samples recorded the highest proportional contribution of meteoric water, and using in situ techniques such as SIMS to target specific domains under a robust petrographic framework will be a prerequisite.

Applications in Sn(-W) deposits

We apply our analytical technique and newly calculated 1000 $\ln \alpha$ of cassiterite-water to nine samples from six Chinese Sn(-W) deposits (Fig. 5A). Obtained $\delta^{18}\text{O}$ values of cassiterite show significant variations both within a single deposit and among deposits (Fig. 5B), which may reflect variable degrees of fluid mixing for Sn(-W) mineralization. We first investigate samples from two individual deposits before discussing the most altered samples in detail, and then discuss samples from all six deposits to yield general trends. For the

Xialonghe Sn(-W) deposit, Yunnan, mineralization is genetically associated with the Xiaolonghe pluton composed of medium-grained to coarse-grained granites. The pluton has a zircon $\delta^{18}\text{O}$ value of $7.80 \pm 0.83\text{‰}$ (Chen et al. 2015). Large variations in the zircon $\delta^{18}\text{O}$ values potentially indicate the presence of inherited zircons, but since it is not expected to bias our estimated $\delta^{18}\text{O}$ values of magmatic fluids significantly, we do not discuss the overdispersion of zircon $\delta^{18}\text{O}$ values further. Assuming primary magmatic fluids reached oxygen isotope equilibrium with the granitic melts during zircon crystallization, it is expected to have a $\delta^{18}\text{O}$ value

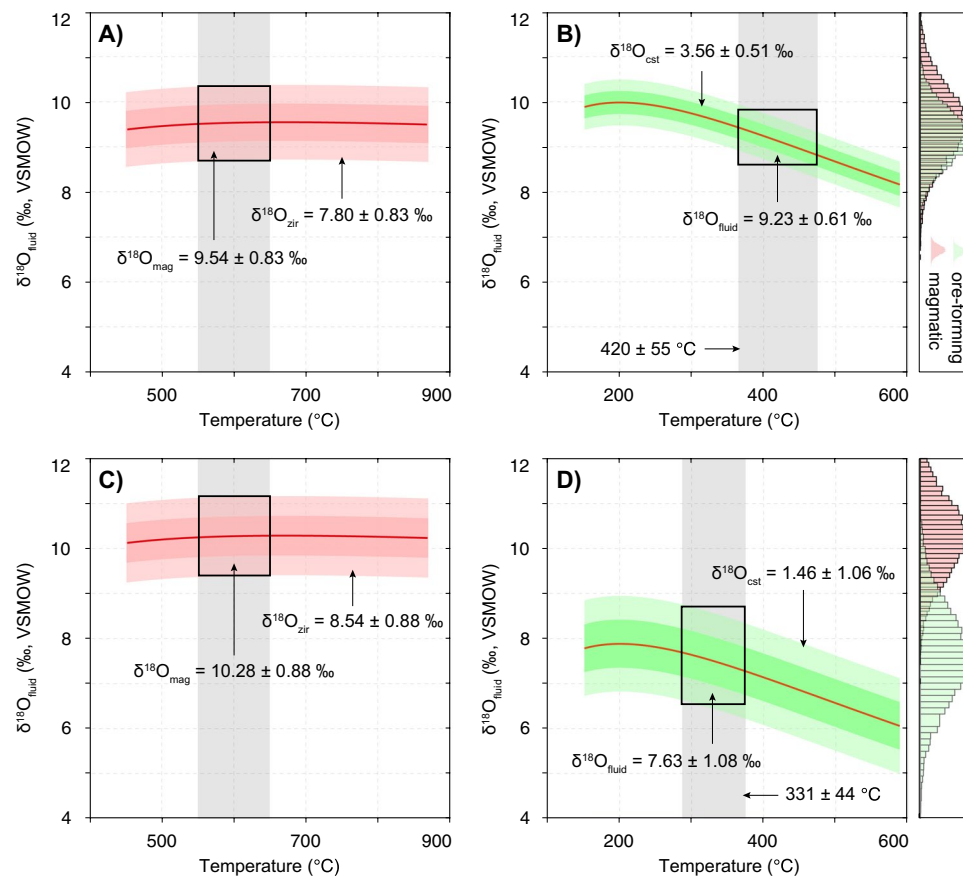


Fig. 6 Constraining the oxygen isotope composition of primary magmatic fluids and ore-forming fluids by analyzing the $\delta^{18}\text{O}$ values of zircon and cassiterite, respectively. **A** Predicting $\delta^{18}\text{O}$ values of primary magmatic fluids at the Xiaolonghe Sn(-W) deposit, Yunnan province; zircon $\delta^{18}\text{O}$ values from SIMS analysis (Chen et al. 2015) are illustrated with 1000 $\ln \alpha$ of zircon-water vs temperature; uncertainties are shown at the 1 and 2 sigma level as the shaded areas; predicted $\delta^{18}\text{O}$ values (at 2 sigma level) of magmatic fluids at $600 \pm 50\text{ °C}$ are shown as a black rectangle. **B** Predicting $\delta^{18}\text{O}$ values of ore-forming fluids at the Xiaolonghe deposit from cassiterite oxygen isotope analysis; 1000 $\ln \alpha$ of cassiterite-water vs temperature with known $\delta^{18}\text{O}$ values of cassiterite from SIMS analysis are illustrated, with uncertainties shown at the 1-2 sigma level as the shaded areas; predicted $\delta^{18}\text{O}$ values (at 2 sigma level) of ore-forming fluids at $420 \pm 55\text{ °C}$ are shown as a black rectangle; ore-forming temperatures are from cassiterite-hosted fluid inclusion assemblages (Cui

et al. 2019). Using a Monte Carlo approach, simulated $\delta^{18}\text{O}$ values of magmatic and ore-forming fluids at the Xiaolonghe deposit are broadly the same as shown at the right side of panel **B**. **C** In a similar fashion to Fig. 6A, $\delta^{18}\text{O}$ values of primary magmatic fluids ($600 \pm 50\text{ °C}$) at the Kafang Sn(-W) deposit, Yunnan province, are calculated; zircon oxygen isotope data are from Cheng et al. (2012). **D** In a similar fashion to Fig. 6B $\delta^{18}\text{O}$ values of ore-forming fluids at the Kafang deposit from cassiterite oxygen isotope analysis at $331 \pm 44\text{ °C}$ are calculated; homogenization temperatures of cassiterite-hosted fluid inclusion assemblages are from previous studies (Cheng et al. 2012; Zhang et al. 2012). Using a Monte Carlo approach, simulated $\delta^{18}\text{O}$ values of magmatic and ore-forming fluids at the Kafang deposit are shown at the right side of panel **D**, which indicates a low degree (i.e., ~12%) involvement of external fluids with low $\delta^{18}\text{O}$ values (see text for details)

of $9.54 \pm 0.83\text{‰}$ at $600 \pm 50\text{ °C}$ (Fig. 6A). Cassiterite samples from the main mineralization stage have $\delta^{18}\text{O}$ values (Fig. 5A) of $3.56 \pm 0.51\text{‰}$ (XLH). Using the temperature ($420 \pm 55\text{ °C}$) estimated from cassiterite-hosted fluid inclusion assemblages (Cui et al. 2019), the oxygen isotope composition of ore-forming fluid during cassiterite precipitation is estimated as $9.23 \pm 0.61\text{‰}$ for sample XLH (Fig. 6B). We would like to highlight here that the accuracy of ore-forming temperatures has very limited effects on estimated $\delta^{18}\text{O}$ values of ore-forming fluids, as expected from the insensitivity between isotope fractionation of cassiterite-water and temperature discussed above. For instance, using temperatures of 520 °C and 320 °C , calculated $\delta^{18}\text{O}$ values of ore-forming fluids are $8.60 \pm 0.62\text{‰}$ and $9.73 \pm 0.56\text{‰}$, respectively, which still are overlapped within uncertainties. For another two samples (RD and DSPK, Fig. 5A–B), estimated $\delta^{18}\text{O}$ values of ore-forming fluids at $420 \pm 55\text{ °C}$ are $8.47 \pm 0.80\text{‰}$ and $8.91 \pm 1.22\text{‰}$ respectively. Within uncertainties, the calculated $\delta^{18}\text{O}$ values of fluids from cassiterite-water systems are essentially the same and show an excellent agreement with $\delta^{18}\text{O}$ values of primary magmatic fluids. Therefore, meteoric water is unlikely to have played a significant role in cassiterite mineralization at the Xiaolonghe deposit.

For the Kafang Sn(-W) deposit, Yunnan, $\delta^{18}\text{O}$ values of cassiterite are $1.46 \pm 1.06\text{‰}$, which are the lowest among all investigated samples except the two altered ones (Fig. 5A–B). Mineralization at Kafang is genetically linked to the Xinshan biotite granite, which has a zircon $\delta^{18}\text{O}$ value of $7.80 \pm 0.83\text{‰}$ (Cheng et al. 2012). The oxygen isotope composition of primary magmatic fluids at Kafang is estimated as $10.28 \pm 0.88\text{‰}$ at $600 \pm 50\text{ °C}$ (Fig. 6C). With ore formation temperatures ($331 \pm 44\text{ °C}$) being constrained by quartz-hosted fluid inclusion assemblages from the main mineralization stage (Cheng et al. 2012; Zhang et al. 2012), the oxygen isotope composition of ore-forming fluids during cassiterite precipitation is estimated as $7.63 \pm 1.08\text{‰}$ (Fig. 6D). This estimated $\delta^{18}\text{O}$ value is slightly lower than that of primary magmatic fluids and requires the involvement of external fluids bearing a depleted oxygen isotope signature. Using the binary mixing model in Fig. 4F, the $\delta^{18}\text{O}$ value and proportional contribution of external water are estimated as $4.81 \pm 2.72\text{‰}$ and $50 \pm 8\%$, respectively. A potential source for this external water is meteoric water which has experienced water–rock interaction with wall rocks with high $\delta^{18}\text{O}$ value (e.g., sedimentary rocks). If we assume the primary meteoric water has a $\delta^{18}\text{O}$ value of -10‰ , then the estimated proportional contribution of primary meteoric water is $\sim 12\%$.

We further investigate samples (V109 and LLSK) from the Lailishan Sn(-W) deposit, Yunnan, which show a high degree of alteration (Fig. 5A). Measured $\delta^{18}\text{O}$ values show considerable variations for both samples, which range from -3.07 to 2.86‰ . While zones with alteration

consistently give low $\delta^{18}\text{O}$ values (peak at $-1.1 \pm 0.4\text{‰}$), areas with low degree of alteration have $\delta^{18}\text{O}$ values of $1.6 \pm 0.4\text{‰}$ (Fig. 5B), and remnants of primary zones have $\delta^{18}\text{O}$ values of up to 3‰ . These features are best explained

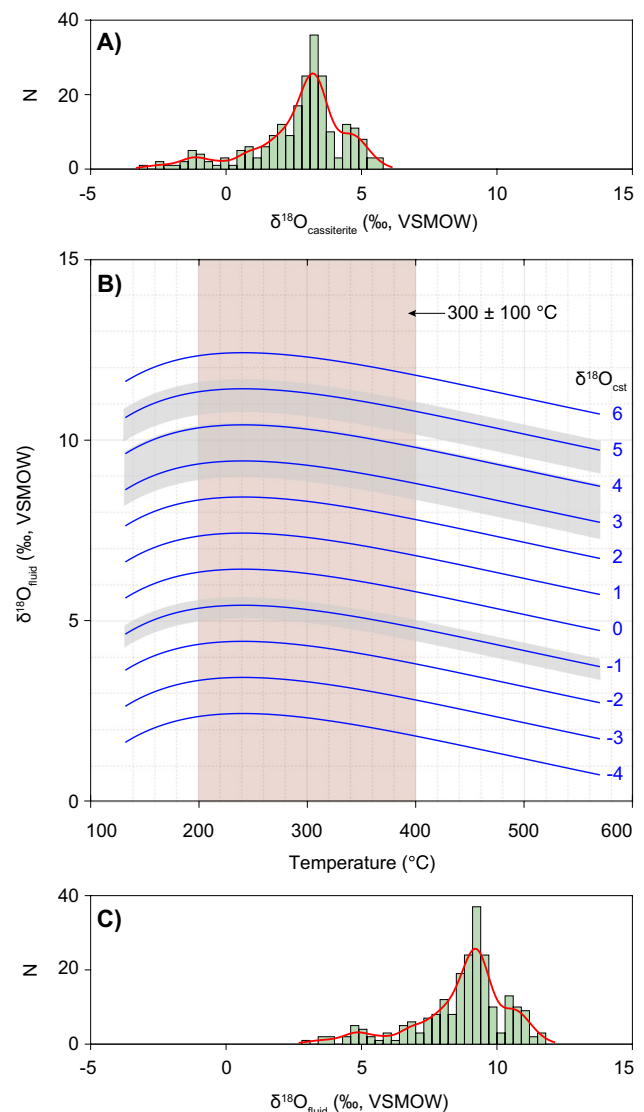


Fig. 7 Oxygen isotope composition of cassiterite and corresponding ore-forming fluids of six Sn(-W) deposits investigated in this study. **A** Histogram of cassiterite $\delta^{18}\text{O}$ values of the six Sn(-W) deposits analyzed in this study; the red curve is the kernel density function which highlights the three major peaks of $\delta^{18}\text{O}$ values of cassiterite at 4.6 ± 0.6 , 3.3 ± 0.8 , and $-1.1 \pm 0.4\text{‰}$. **B** $1000 \ln \alpha$ of cassiterite-water vs temperature is given, with three major peaks of $\delta^{18}\text{O}$ values of cassiterite from the six Sn(-W) deposits being illustrated as shaded areas (uncertainties at 2 sigma level). **C** At a temperature of $300 \pm 100\text{ °C}$, predicted $\delta^{18}\text{O}$ values of ore-forming fluids are shown as histogram with peaks of 10.6 ± 1.2 , 9.3 ± 1.2 , and $4.9 \pm 1.1\text{‰}$; these estimates predominately show a magmatic affinity ($9\text{--}11\text{‰}$), with no to low degree involvements ($\sim 0\text{--}10\text{‰}$) of fluids with low $\delta^{18}\text{O}$ values (e.g., meteoric water); we would like to highlight here that obtaining the $\delta^{18}\text{O}$ values of ore-forming fluids from cassiterite is not sensitive to temperature estimates (see text for further discussion)

by a two-stage process, where cassiterite grains were firstly formed with a magmatic affinity, and then experienced alteration by fluids bearing low $\delta^{18}\text{O}$ values. This highlights that cassiterite could record multiple stages of fluid evolution with the preservation of primary oxygen isotope signature, and using in situ techniques with detailed petrographic study is critical to reveal a more comprehensive history.

With individual deposits having been discussed, now we consider general trends of cassiterite $\delta^{18}\text{O}$ values from all studied deposits. Pooling the data together, 221 oxygen isotope analyses of cassiterite by SIMS define three distinct peaks at 4.6 ± 0.6 , 3.3 ± 0.8 , and $-1.1 \pm 0.4\text{‰}$ (Fig. 7A). We use $300 \pm 100\text{ °C}$ as the best estimated temperature (Fig. 7B) for cassiterite precipitation, and calculated $\delta^{18}\text{O}$ values of ore-forming fluids also show considerable variations with peaks at 10.6 ± 1.2 , 9.3 ± 1.2 , and $4.9 \pm 1.1\text{‰}$ (Fig. 7C). As discussed above, $1000 \ln \alpha$ of cassiterite-water is insensitive to temperature over a wide range of temperatures (Fig. 4C); hence, the calculated $\delta^{18}\text{O}$ values of ore-forming fluids are robust despite of temperature fluctuations. Our results indicate that most cassiterite, and by inference, tin mineralization, was crystallized from fluids with a magmatic affinity (e.g., 9–11‰, Fig. 7C), with variable but consistently low degree involvements (~0–10%) of meteoric water. Mixing magmatic fluids and meteoric water has been proposed as a primary driver to promote metal deposition in Sn(-W) deposits. While mixing induced cooling certainly could play a significant role in this regard (Legros et al. 2019; Xiong et al. 2019; Liu et al. 2020; Harlaux et al. 2021), most samples studied here seems do not require the involvement of meteoric water. Traditional models suggest that meteoric water plays an important role in triggering metals precipitation in Sn-W deposits, hence, our cassiterite oxygen isotope analysis calls for a reassessment on the extent and role of meteoric water in these systems.

Since the oxygen isotope fractionation between cassiterite and water is not sensitive to temperature (Fig. 4C), the observed variations in cassiterite $\delta^{18}\text{O}$ values are best explained by fluctuations in $\delta^{18}\text{O}$ values of ore-forming fluids. Possible mechanisms that could account for these variable $\delta^{18}\text{O}$ values of ore-forming fluids include fluid mixing and water-rock interaction. Taking advantage of the high spatial resolution of ion microprobe analysis, it is possible to reveal a more complete picture of the interaction between magmatic fluid and meteoric water and wallrocks during ore formation, and we expect to achieve a deeper and more detailed understanding of how the sources, dynamics and evolution of hydrothermal fluids control Sn(-W) mineralization.

Conclusion

Our robust evaluation demonstrates a lack of crystallographic orientation effect on cassiterite oxygen isotope analysis by ion microprobe at the current analytical precision (e.g., ~0.2–0.3‰).

Along with the Yongde-Cst, a mega-crystal of cassiterite which has been developed as a matrix-matched reference material for oxygen isotope analysis, we have paved the way for cassiterite oxygen isotope analysis by ion microprobe. The recommended $\delta^{18}\text{O}$ value for the Yongde-Cst is $1.36 \pm 0.16\text{‰}$, as determined by gas source isotope ratio mass spectrometry. We further calculated the temperature-dependent isotope fractionation between quartz and cassiterite, which is given by the equation of $1.259 \times 10^6/T^2 + 8.15 \times 10^3/T - 4.72$ (T is temperature in Kelvin); hence, the fractionation between cassiterite and water is given by $2.94 \times 10^6/T^2 - 11.45 \times 10^3/T + 4.72$ (T is temperature in Kelvin). A sensitive response of the oxygen isotope fractionation between quartz and cassiterite to temperature makes cassiterite-quartz an excellent oxygen isotope thermometer, as described by the equation of $T(\text{°C}) = 2427 \times (\delta^{18}\text{O}_{\text{qtz}} - \delta^{18}\text{O}_{\text{cst}})^{-0.4326} - 492.4$. Current analytical precision of SIMS $\delta^{18}\text{O}$ is ~0.2–0.3‰; this will bring an uncertainty of $\pm 10\text{ °C}$ for temperatures estimated from the quartz-cassiterite oxygen isotope thermometer. We further developed a conceptual model to derive $\delta^{18}\text{O}$ and temperature of ore-forming fluids, as well as the $\delta^{18}\text{O}$ and proportional contribution of meteoric water in magmatic-hydrothermal systems, with the $\delta^{18}\text{O}$ values of zircon, cassiterite, and quartz as inputs. We eventually applied SIMS oxygen isotope analysis to cassiterite samples from six deposits, which revealed significant fluctuations in $\delta^{18}\text{O}$ values both within a single deposit and between deposits. The predicted $\delta^{18}\text{O}$ of ore-forming fluids bears a strong magmatic affinity, with variable and mostly no to low degree (~0–10%) involvements of meteoric water. Our results presented here invite a reassessment on the extent and role of meteoric water in Sn-W deposits, and highlight the fact that in situ oxygen isotope analysis of cassiterite is a very promising tool for tracing the sources and evolutionary processes of ore-forming fluids.

Supplementary Information The online version contains supplementary material available at <https://doi.org/10.1007/s00126-021-01068-x>.

Acknowledgements We thank Shun Wang for providing the Yongde-Cst. We thank Prof Ian Williams and Dr Patrick Carr for their constructive comments and suggestions that significantly improved the presentation and clarity of this manuscript. We extend our gratitude to Prof David Dolejs and Prof Bernd Lehmann for their informative suggestions and professional editorial handling.

Funding This research is supported by National Key Research and Development Program of China (2018YFA0702600), National Natural Science Foundation of China (42022022), and Pioneer Hundred Talents Program of Chinese Academy of Sciences and CNNC Science Fund for Talented Young Scholars (QNYC2019-2).

References

- Bigeleisen J, Mayer MG (1947) Calculation of equilibrium constants for isotopic exchange reactions. *J Chem Phys* 15:261–267. <https://doi.org/10.1063/1.1746492>

- Blevin PL, Chappell BW (1995) Chemistry, origin, and evolution of mineralized granites in the Lachlan fold belt, Australia: the metallogeny of I- and S-type granites. *Econ Geol Bull Soc* 90:1604–1619. <https://doi.org/10.2113/gsecongeo.90.6.1604>
- Bodnar RJ, Lecumberri-Sanchez P, Moncada D, Steele-MacInnis M (2014) 13.5 - Fluid inclusions in hydrothermal ore deposits. In: Turekian HDHK (ed) *Treatise on geochemistry* (Second Edition). Elsevier, Oxford, pp 119–142
- Breiter K, Skoda R, Uher P (2007) Nb-Ta-Ti-W-Sn-oxide minerals as indicators of a peraluminous P- and F-rich granitic system evolution: Podlesi, Czech Republic. *Mineral Petrol* 91:225–248. <https://doi.org/10.1007/s00710-007-0197-1>
- Cai MH, Mao JW, Ting L, Pirajno F, Huang HL (2007) The origin of the Tongkeng-Changpo tin deposit, Dachang metal district, Guangxi, China: clues from fluid inclusions and He isotope systematics. *Miner Deposita* 42:613–626. <https://doi.org/10.1007/s00126-007-0127-5>
- Cao HW, Zou H, Zhang YH, Zhang ST, Zheng L, Zhang LK, Tang L, Pei QM (2016) Late Cretaceous magmatism and related metallogeny in the Tengchong area: evidence from geochronological, isotopic and geochemical data from the Xiaolonghe Sn deposit, western Yunnan, China. *Ore Geol Rev* 78:196–212. <https://doi.org/10.1016/j.oregeorev.2016.04.002>
- Carr P, Norman MD, Bennett VC, Blevin PL (2020) Tin enrichment in magmatic-hydrothermal environments associated with cassiterite mineralization at Ardlethan Eastern Australia: insights from Rb-Sr and Sm-Nd Isotope Compositions in Tourmaline. *Econ Geol*. <https://doi.org/10.5382/econgeo.4774>
- Carr PA, Norman MD, Bennett VC (2017) Assessment of crystallographic orientation effects on secondary ion mass spectrometry (SIMS) analysis of cassiterite. *Chem Geol* 467:122–133. <https://doi.org/10.1016/j.chemgeo.2017.08.003>
- Chen XC, Hu RZ, Bi XW, Li HM, Lan JB, Zhao CH, Zhu JJ (2014) Cassiterite LA-MC-ICP-MS U/Pb and muscovite Ar-40/Ar-39 dating of tin deposits in the Tengchong-Lianghe tin district, NW Yunnan, China. *Miner Deposita* 49:843–860. <https://doi.org/10.1007/s00126-014-0513-8>
- Chen XC, Hu RZ, Bi XW, Zhong H, Lan JB, Zhao CH, Zhu JJ (2015) Petrogenesis of metaluminous A-type granitoids in the Tengchong-Lianghe tin belt of southwestern China: evidences from zircon U-Pb ages and Hf-O isotopes, and whole-rock Sr-Nd isotopes. *Lithos* 212:93–110. <https://doi.org/10.1016/j.lithos.2014.11.010>
- Cheng YB, Mao JW, Rusk B, Yang ZX (2012) Geology and genesis of Kafang Cu-Sn deposit, Gejiu district, SW China. *Ore Geol Rev* 48:180–196. <https://doi.org/10.1016/j.oregeorev.2012.03.004>
- Chi G, Diamond LW, Lu H, Lai J, Chu H (2021) Common problems and pitfalls in fluid inclusion study: a review and discussion. *Minerals* 11:7
- Clayton RN, Mayeda TK, Oneil JR (1972) Oxygen isotope-exchange between quartz and water. *J Geophys Res* 77:3057–4000. <https://doi.org/10.1029/JB077i017p03057>
- Cooke DR, Hollings P, Wilkinson JJ, Tosdal RM (2014) 13.14 - Geochemistry of porphyry deposits. In: Turekian HDHK (ed) *Treatise on geochemistry* (Second Edition). Elsevier, Oxford, pp 357–381
- Cui XL, Wang QF, Deng J, Wu HY, Shu QH (2019) Genesis of the Xiaolonghe quartz vein type Sn deposit, SW China: insights from cathodoluminescence textures and trace elements of quartz, fluid inclusions, and oxygen isotopes. *Ore Geol Rev* 111. UNSP 10292910.1016/j.oregeorev.2019.05.015
- D'Errico ME, Lackey JS, Surpless BE, Loewy SL, Wooden JL, Barnes JD, Strickland A, Valley JW (2012) A detailed record of shallow hydrothermal fluid flow in the Sierra Nevada magmatic arc from low- $\delta^{18}\text{O}$ skarn garnets. *Geology* 40:763–766. <https://doi.org/10.1130/g33008.1>
- Fekete S, Weis P, Driesner T, Bouvier AS, Baumgartner L, Heinrich CA (2016) Contrasting hydrological processes of meteoric water incursion during magmatic-hydrothermal ore deposition: an oxygen isotope study by ion microprobe. *Earth Planet Sci Lett* 451:263–271. <https://doi.org/10.1016/j.epsl.2016.07.009>
- Feng L, Li H, Li T (2020) Potential reference materials for hematite oxygen isotope analysis. *Minerals* 10:987
- Fu M, Changkakoti A, Krouse HR, Gray J, Kwak TAP (1991) An oxygen, hydrogen, sulfur, and carbon isotope study of carbonate-replacement (skarn) tin deposits of the Dachang tin field, China. *Econ Geol Bull Soc* 86:1683–1703. <https://doi.org/10.2113/gsecongeo.86.8.1683>
- Giannozzi P, Baroni S, Bonini N, Calandra M, Car R, Cavazzoni C, Ceresoli D, Chiarotti GL, Cococcioni M, Dabo I, Dal Corso A, de Gironcoli S, Fabris S, Fratesi G, Gebauer R, Gerstmann U, Gougoussis C, Kokalj A, Lazzeri M, Martin-Samos L, Marzari N, Mauri F, Mazzarello R, Paolini S, Pasquarello A, Paulatto L, Sbraccia C, Scandolo S, Sclauzero G, Seitsonen AP, Smogunov A, Umari P, Wentzcovitch RM (2009) QUANTUM ESPRESSO: a modular and open-source software project for quantum simulations of materials. *J Phys Condens Matter* 21:395502. <https://doi.org/10.1088/0953-8984/21/39/395502>
- Guo J, Zhang RQ, Li CY, Sun WD, Hu YB, Kang DM, Wu JD (2018a) Genesis of the Gaosong Sn-Cu deposit, Gejiu district, SW China: constraints from in situ LA-ICP-MS cassiterite U-Pb dating and trace element fingerprinting. *Ore Geol Rev* 92:627–642. <https://doi.org/10.1016/j.oregeorev.2017.11.033>
- Guo J, Zhang RQ, Sun WD, Ling MX, Hu YB, Wu K, Luo M, Zhang LC (2018b) Genesis of tin-dominant polymetallic deposits in the Dachang district, South China: insights from cassiterite U-Pb ages and trace element compositions. *Ore Geol Rev* 95:863–879. <https://doi.org/10.1016/j.oregeorev.2018.03.023>
- Harlaux M, Kouzmanov K, Gialli S, Marger K, Bouvier A-S, Baumgartner LP, Rielli A, Dini A, Chauvet A, Kalinaj M, Fontboté L (2021) Fluid mixing as primary trigger for cassiterite deposition: evidence from in situ $\delta^{18}\text{O}$ - $\delta^{11}\text{B}$ analysis of tourmaline from the world-class San Rafael tin (-copper) deposit, Peru. *Earth Planet Sci Lett* 563. <https://doi.org/10.1016/j.epsl.2021.116889>
- Hu GX, Clayton RN, Polyakov VB, Mineev SD (2005) Oxygen isotope fractionation factors involving cassiterite (SnO₂): II. Determination by direct isotope exchange between cassiterite and calcite. *Geochim Cosmochim Acta* 69:1301–1305. <https://doi.org/10.1016/j.gca.2004.09.002>
- Huang F, Chen LJ, Wu ZQ, Wang W (2013) First-principles calculations of equilibrium Mg isotope fractionations between garnet, clinopyroxene, orthopyroxene, and olivine: implications for Mg isotope thermometry. *Earth Planet Sci Lett* 367:61–70. <https://doi.org/10.1016/j.epsl.2013.02.025>
- Huberty JM, Kita NT, Kozdon R, Heck PR, Fournelle JH, Spicuzza MJ, Xu H, Valley JW (2010) Crystal orientation effects in $\delta^{18}\text{O}$ for magnetite and hematite by SIMS. *Chem Geol* 276:269–283. <https://doi.org/10.1016/j.chemgeo.2010.06.012>
- Isa J, Kohl IE, Liu MC, Wasson JT, Young ED, McKeegan KD (2017) Quantification of oxygen isotope SIMS matrix effects in olivine samples: correlation with sputter rate. *Chem Geol* 458:14–21. <https://doi.org/10.1016/j.chemgeo.2017.03.020>
- Kita NT, Ushikubo T, Fu B, Valley JW (2009) High precision SIMS oxygen isotope analysis and the effect of sample topography. *Chem Geol* 264:43–57. <https://doi.org/10.1016/j.chemgeo.2009.02.012>

- Legros H, Richard A, Tarantola A, Kouzmanov K, Mercadier J, Vennemann T, Marignac C, Cuney M, Wang RC, Charles N, Bailly L, Lespinasse MY (2019) Multiple fluids involved in granite-related W-Sn deposits from the world-class Jiangxi province (China). *Chem Geol* 508:92–115. <https://doi.org/10.1016/j.chemgeo.2018.11.021>
- Lehmann B (1982) Metallogeny of tin: magmatic differentiation versus geochemical heritage. *Econ Geol* 77:50–59
- Li XH, Li WX, Wang XC, Li QL, Liu Y, Tang GQ (2009) Role of mantle-derived magma in genesis of early Yanshanian granites in the Nanling Range, South China: in situ zircon Hf-O isotopic constraints. *Sci China Ser D* 52:1262–1278. <https://doi.org/10.1007/s11430-009-0117-9>
- Li Y, Li XH, Selby D, Li JW (2018) Pulsed magmatic fluid release for the formation of porphyry deposits: tracing fluid evolution in absolute time from the Tibetan Qulong Cu-Mo deposit. *Geology* 46:7–10. <https://doi.org/10.1130/G39504.1>
- Li Y, Zhang S, Hobbs R, Caiado C, Sproson AD, Selby D, Rooney AD (2019) Monte Carlo sampling for error propagation in linear regression and applications in isochron geochronology. *Sci Bull* 64:189–197. <https://doi.org/10.1016/j.scib.2018.12.019>
- Li Y, Tang G-Q, Liu Y, He S, Chen B, Li Q-L, Li X-H (2021) Revisiting apatite SIMS oxygen isotope analysis and Qinghu-AP reference material. *Chem Geol* 582:120445. <https://doi.org/10.1016/j.chemgeo.2021.120445>
- Liang T, Wang DH, Hou KJ, Li HQ, Huang HM, Cai MH, Wang DM (2011) LA-MC-ICP-MS zircon U-Pb dating of Longxianggai pluton in Dachang of Guangxi and its geological significance. *Acta Petrol Sin* 27:1624–1636
- Liu P, Mao JW, Jian W, Mathur R (2020) Fluid mixing leads to main-stage cassiterite precipitation at the Xiling Sn polymetallic deposit, SE China: evidence from fluid inclusions and multiple stable isotopes (H-O-S). *Miner Deposita* 55:1233–1246. <https://doi.org/10.1007/s00126-019-00933-0>
- Perdew JP, Zunger A (1981) Self-interaction correction to density-functional approximations for many-electron systems. *Phys Rev B* 23:5048–5079. <https://doi.org/10.1103/PhysRevB.23.5048>
- Peres P, Kita NT, Valley JW, Fernandes F, Schuhmacher M (2013) New sample holder geometry for high precision isotope analyses. *Surf Interface Anal* 45:553–556. <https://doi.org/10.1002/sia.5061>
- Polyakov VB, Mineev SD, Clayton RN, Hu G, Gurevich VM, Khramov DA, Gavrichev KS, Gorbunov VE, Golushina LN (2005) Oxygen isotope fractionation factors involving cassiterite (SnO₂): I. Calculation of reduced partition function ratios from heat capacity and X-ray resonant studies. *Geochim Cosmochim Acta* 69:1287–1300. <https://doi.org/10.1016/j.gca.2004.08.034>
- Richet P, Bottinga Y, Javoy M (1977) A review of hydrogen, carbon, nitrogen, oxygen, sulphur, and chlorine stable isotope fractionation among gaseous molecules. *Annu Rev Earth Planet Sci* 5:65–110. <https://doi.org/10.1146/annurev.ea.05.050177.000433>
- Schmitt AK, Zack T (2012) High-sensitivity U-Pb rutile dating by secondary ion mass spectrometry (SIMS) with an O₂⁺ primary beam. *Chem Geol* 332–333:65–73. <https://doi.org/10.1016/j.chemgeo.2012.09.023>
- Scicchitano MR, Rubatto D, Hermann J, Majumdar AS, Putnis A (2018) Oxygen isotope analysis of olivine by ion microprobe: matrix effects and applications to a serpentinized dunite. *Chem Geol* 499:126–137. <https://doi.org/10.1016/j.chemgeo.2018.09.020>
- Sharp ZD, Gibbons JA, Maltsev O, Atudorei V, Pack A, Sengupta S, Shock EL, Knauth LP (2016) A calibration of the triple oxygen isotope fractionation in the SiO₂-H₂O system and applications to natural samples. *Geochim Cosmochim Acta* 186:105–119. <https://doi.org/10.1016/j.gca.2016.04.047>
- Shulaker DZ, Schmitt AK, Zack T, Bindeman I (2015) In-situ oxygen isotope and trace element geothermometry of rutilated quartz from Alpine fissures. *Am Miner* 100:915–925. <https://doi.org/10.2138/am-2015-4961>
- Tang GQ, Li XH, Li QL, Liu Y, Ling XX, Yin QZ (2015) Deciphering the physical mechanism of the topography effect for oxygen isotope measurements using a Cameca IMS-1280 SIMS. *J Anal at Spectrom* 30:950–956. <https://doi.org/10.1039/c4ja00458b>
- Tang GQ, Liu Y, Li QL, Feng LJ, Wei GJ, Su W, Li Y, Ren GH, Li XH (2020) New natural and fused quartz reference materials for oxygen isotope microanalysis. *Atomic Spectrosc* 41:188–193. <https://doi.org/10.46770/As.2020.05.002>
- Taylor R, Clark C, Reddy SM (2012) The effect of grain orientation on secondary ion mass spectrometry (SIMS) analysis of rutile. *Chem Geol* 300:81–87. <https://doi.org/10.1016/j.chemgeo.2012.01.013>
- Trail D, Bindeman IN, Watson EB, Schmitt AK (2009) Experimental calibration of oxygen isotope fractionation between quartz and zircon. *Geochim Cosmochim Acta* 73:7110–7126. <https://doi.org/10.1016/j.gca.2009.08.024>
- Troullier N, Martins JL (1991) Efficient pseudopotentials for plane-wave calculations. *Phys Rev B Condens Matter* 43:1993–2006. <https://doi.org/10.1103/physrevb.43.1993>
- Urey HC (1947) The thermodynamic properties of isotopic substances. *J Chem Soc* 562–581. <https://doi.org/10.1039/jr9470000562>
- Valley JW (2003) Oxygen isotopes in zircon. *Rev Mineral Geochem* 53:343–385. <https://doi.org/10.2113/0530343>
- Vanderbilt D (1990) Soft self-consistent pseudopotentials in a generalized eigenvalue formalism. *Phys Rev B Condens Matter* 41:7892–7895. <https://doi.org/10.1103/physrevb.41.7892>
- Wang W, Dong G, Sun Z, Dong P, Pan Y, Ketchaya YB, Lemdjou YB, Geng J (2020) The genesis of Eocene granite-related Lailishan tin deposit in western Yunnan, China: Constraints from geochronology, geochemistry, and S-Pb-H-O isotopes. *Geol J* 56:508–524. <https://doi.org/10.1002/gj.3928>
- Wang WZ, Zhou C, Qin T, Kang JT, Huang SC, Wu ZQ, Huang F (2017) Effect of Ca content on equilibrium Ca isotope fractionation between orthopyroxene and clinopyroxene. *Geochim Cosmochim Acta* 219:44–56. <https://doi.org/10.1016/j.gca.2017.09.022>
- Wentzcovitch RM (1991) Invariant molecular-dynamics approach to structural phase transitions. *Phys Rev B Condens Matter* 44:2358–2361. <https://doi.org/10.1103/physrevb.44.2358>
- Wilkinson JJ (2001) Fluid inclusions in hydrothermal ore deposits. *Lithos* 55:229–272. [https://doi.org/10.1016/S0024-4937\(00\)00047-5](https://doi.org/10.1016/S0024-4937(00)00047-5)
- Wood SA, Samson IM (2000) The hydrothermal geochemistry of tungsten in granitoid environments: I. Relative solubilities of ferberite and scheelite as a function of T, P, pH, and mNaCl. *Econ Geol* 95:143–182. <https://doi.org/10.2113/gsecongeo.95.1.143>
- Xiong YQ, Shao YJ, Mao JW, Wu SC, Zhou HD, Zheng MH (2019) The polymetallic magmatic-hydrothermal Xiangdong and Dalong systems in the W-Sn-Cu-Pb-Zn-Ag Dengfuxian orefield, SE China: constraints from geology, fluid inclusions, H-O-S-Pb isotopes, and sphalerite Rb-Sr geochronology. *Miner Deposita* 54:1101–1124. <https://doi.org/10.1007/s00126-019-00863-x>
- Yao Y, Chen J, Lu JJ, Wang RC, Zhang RQ (2014) Geology and genesis of the Hehuaping magnesian skarn-type cassiterite-sulfide deposit, Hunan Province, Southern China. *Ore Geol Rev* 58:163–184. <https://doi.org/10.1016/j.oregeorev.2013.10.012>
- Zhang J, Mao JW, Cheng YB, Li XL (2012) Mineralization process of the Kafang tin-copper deposit in the Gejiu district, Yunnan Province: constraints from fluid inclusion. *Acta Petrol Sin* 28:166–182
- Zhang L-G, Liu J, Chen Z, Zhou H (1994) Experimental investigations of oxygen isotope fractionation in cassiterite and wolframite. *Econ Geol* 89:150–157. <https://doi.org/10.2113/gsecongeo.89.1.150>
- Zhang LP, Zhang RQ, Hu YB, Liang JL, Ouyang ZX, He JJ, Chen YX, Guo J, Sun WD (2017) The formation of the Late Cretaceous Xishan Sn-W deposit, South China: geochronological and


geochemical perspectives. *Lithos* 290:253–268. <https://doi.org/10.1016/j.lithos.2017.08.013>

Zhang R-Q, Lu J-J, Wang R-C, Yang P, Zhu J-C, Yao Y, Gao J-F, Li C, Lei Z-H, Zhang W-L, Guo W-M (2015) Constraints of in situ zircon and cassiterite U-Pb, molybdenite Re-Os and muscovite ^{40}Ar - ^{39}Ar ages on multiple generations of granitic magmatism and related W-Sn mineralization in the Wangxianling area, Nanling Range, South China. *Ore Geol Rev* 65:1021–1042. <https://doi.org/10.1016/j.oregeorev.2014.09.021>

Zheng Y-F (1991) Calculation of oxygen isotope fractionation in metal oxides. *Geochim Cosmochim Acta* 55:2299–2307

Publisher's note Springer Nature remains neutral with regard to jurisdictional claims in published maps and institutional affiliations.

Authors and Affiliations

Yang Li¹  · Sheng He² · Rong-Qing Zhang³ · Xian-Wu Bi⁴ · Lian-Jun Feng¹ · Guo-Qiang Tang¹ · Wen-Zhong Wang^{5,6} · Fang Huang⁷ · Xian-Hua Li¹

¹ State Key Laboratory of Lithospheric Evolution, Institute of Geology and Geophysics, Chinese Academy of Sciences, Beijing 100029, China

² Beijing Research Institute of Uranium Geology, Beijing 100029, China

³ State Key Laboratory for Mineral Deposits Research, Nanjing University, Nanjing 210046, China

⁴ State Key Laboratory of Ore Deposit Geochemistry, Institute of Geochemistry, Chinese Academy of Sciences, Guiyang 550081, China

⁵ Department of Earth Sciences, University College London, London WC1E 6BT, UK

⁶ Earth and Planets Laboratory, Carnegie Institution for Science, Washington, DC 20015, USA

⁷ Laboratory of Seismology and Physics of Earth's Interior, School of Earth and Space Sciences, University of Science and Technology of China, Hefei 230026, Anhui, China